The Pennsylvania State University

The Graduate School

Department of Aerospace Engineering

EFFICIENT CFD APPROACHES FOR COAXIAL ROTOR SIMULATIONS

A Thesis in

Aerospace Engineering

by

Jason K. Cornelius

Submitted in Partial Fulfillment
of the Requirements
for the Degree of

Master of Science

May 2019

The thesis of Jason K. Cornelius was reviewed and approved* by the following:

Sven Schmitz
Associate Professor, Aerospace Engineering
Thesis Advisor

Michael P. Kinzel
Assistant Professor, Mechanical and Aerospace Engineering

Amy R. Pritchett
Department Head, Aerospace Engineering

*Signatures are on file in the Graduate School

ABSTRACT

The advent of small-scale multicopter aircraft, including quad- and octocopter configurations, has opened the door to potential cost-effective vertical flight technology. These aircraft are intended to be used in applications such as public transportation, recreational products, commercial vehicles, military technologies, and even extraterrestrial planetary exploration. As the demand for these aircraft continues to rise, analysis capabilities for their design and performance prediction become increasingly useful. Complex problems such as rotor-rotor interactions call for high-fidelity prediction tools, but conventional approaches using these tools have immense computational demand that commonly leads to running a simulation on the order of days to weeks.

In this work, two separate computational fluid dynamics approaches, one blade-resolved and one blade-modeled, are studied using the STAR-CCM+ and RotCFD programs to analyze a coaxial rotor configuration. The blade-resolved approach, which will be referred to as the mixing-plane model, involves the development of a novel modeling method for rotorcraft CFD. The mixing-plane model allows for (1) a smaller cell count due to the ability to utilize periodic boundaries which nearly halve the cell count in the context of a RANS CFD model, (2) enabling the usage of steady algorithms for the rotor solution, (3) and not demanding a highly-resolved rotor wake. The results are compared to that of a baseline time-accurate model, i.e. the current state-of-the-art. The methodology, benchmarking process, and preliminary results indicate that the new modeling approach has potential for future analyses to support engineering design. They reduce the computational cost by more than two orders-of-magnitude over the conventional solution method while still providing a CFD resolved solution that is within 2% of rotor thrust, power, and figure of merit in hover.

The physics behind the implementation of the mixing-plane method breaks down in edge-

wise flight where the model does not compare as well. Since a highly efficient approach for a coaxial rotor in edge-wise flight was desired, a blade-modeled approach was also explored. The blade-element method was used for this second modeling approach. It represents the rotors with a rotating line of momentum sources that imparts momentum into the flow-field based on the local CFD resolved inflow and the appropriate airfoil performance table. This method is even faster than the first approach discussed, since it is blade-modeled, and still yields rotor performance calculations that agree with time-accurate, i.e. state-of-the-art, simulations.

A model incorporating this blade-element method was developed and then used to analyze a coaxial rotor configuration. The coaxial rotor is analyzed in hover, edge-wise flight, and axial climb. The blade-element model was found to provide mid-fidelity results in a fraction of the time as the conventional baseline approach. The model also opens the door for the average user, with only a graphics-card equipped computer, to rotorcraft simulations with CFD resolved inflows and wakes.

TABLE OF CONTENTS

LIST OF FIGURES

LIST OF TABLES

NOMENCLATURE

AOA	Angle of Attack	degrees
BTP	Blade Tip Pitch	degrees
C_D	Three-Dimensional Blade Drag Coefficient	$\frac{D}{\frac{1}{2}\rho U_\infty^2 A}$
C_d	Two-Dimensional Drag Coefficient	$\frac{d}{\frac{1}{2}\rho U_\infty^2 A}$
C_L	Three-Dimensional Blade Drag Coefficient	$\frac{L}{\frac{1}{2}\rho U_\infty^2 c}$
C_l	Two-Dimensional Drag Coefficient	$\frac{l}{\frac{1}{2}\rho U_\infty^2 c}$
C_p	Two-Dimensional Blade Pressure Coefficient	$\frac{p}{\frac{1}{2}\rho U_\infty^2}$
P	Reference Pressure	Pa
M	Mach Number	$\frac{U_\infty}{a}$
Re	Reynolds Number	$\frac{\rho U_\infty c}{\mu}$
x, y, z	Cartesian Coordinate System	m
x-axis	Stream wise positive	m
y-axis	Upward positive	m
z-axis	Span-wise positive	m
ρ	Density	kg/m^3
ν	Kinematic Viscosity	m^2/s
μ	Dynamic Viscosity	$kg*s/m^2$
p	Static pressure	N/m^2

ABBREVIATIONS

2D	Two-Dimensional
3D	Three-Dimensional
CAD	Computer Aided Design
CFD	Computational Fluid Dynamics
CSD	Computational Structural Dynamics
FM	Figure of Merit
Gb	Gigabytes
GPU	Graphics Processing Unit
GRS	Grid Resolution Study
GUI	Graphical User Interface
k-ε	K-Epsilon Turbulence Model
k-Ω	K-Omega Turbulence Model
LE	Leading Edge
LRTA	Large Rotor Test Apparatus
NACA	National Advisory Committee for Aeronautics
NASA	National Aeronautics and Space Administration
NAS	NASA Advanced Supercomputing Division
NFAC	National Full-Scale Aerodynamics Complex
NS	Navier-Stokes
RAM	Random Access Memory
RANS	Reynolds-Averaged Navier-Stokes
RPM	Revolutions per Minute

SA	Spalart-Allmaras Turbulence Model
TE	Trailing Edge
UAS	Unmanned Aerial Systems
VRAM	Video Random Access Memory
VTOL	Vertical Take-Off and Landing

ACKNOWLEDGEMENTS

I would like to thank Dr. Sven Schmitz for first getting me involved in this research endeavor, and more importantly, for taking me under his wing when I was only a junior at Penn State. Also, a very big thank you to Dr. Michael Kinzel, who first brought the mixing-plane approach to my attention and assisted me greatly with the technical details throughout the research. Additionally, my lab mates Drs. Adam Lavely, Bernardo Vieira and Amandeep Premi, as well as Regis Thedin and Ethan Corle, were all instrumental in my success with developing the computational models presented. I'll also take the opportunity to thank Dr. George Lesieutre, Dr. Susan Stewart, Professor Rick Auhl, Amy Custer, and Maria Beaty of the Aerospace Department for their continued support and guidance over the years. Also, a big thank you to Dr. Amy Pritchett for her help and feedback in improving the presentation of this work.

A special thanks to Larry Young and Witold Koning of the NASA Ames Research Center's Rotorcraft Aeromechanics Branch. Larry assisted and guided me in a full-vehicle analysis of our aircraft, while providing his wealth of insight on planetary exploration vehicles. Witold also helped in learning and applying the RotCFD toolset to the problems at hand. Additionally, many thanks to Dr. Ganesh Rajagopalan and William Polzin of Sukra-Helitek for their assistance in obtaining and installing academic licenses of the RotCFD program. Along those lines, a special thanks to Kirk Heller of the Penn State Aerospace Department, who spent countless hours helping me get the software running on my computational resources at Penn State.

There were also a few folks within the broader College of Engineering who helped me immensely along the way. I credit much of my success at Penn State to a great personal friend of mine, Dr. Xinli Wu, whose mentorship has pushed me to be the very best I can be in all aspects of life. His travel-based study abroad course, "Impact of Culture on Engineering in China," first

stirred my interest in developing a global perspective, which has flourished into several trips abroad to multiple countries. My involvement in the College of Engineering Research Initiative's (CERI) Research Experience for Undergraduates (REU) program with program leaders Erin Hostetler and Cynthia Reed was also a key driver early on in the work I have completed.

Three additional highly influential mentors, who no doubt guided me at different stages toward a research career in vertical lift, are Dr. Edward Smith of Penn State, Dr. Albert Brand of Bell Helicopter, and Dr. William Warmbrodt of the NASA Ames Research Center. I consider all three personal mentors and have only the utmost appreciation for their guidance.

Lastly, I would like to thank all my friends and family for their encouragement throughout my educational pursuits. The level of support has been nothing short of extraordinary.

There are countless more people that have helped me at one point or another along this journey that is still moving with great speed. Although I can't possibly list them all, their influence has nonetheless helped me move closer towards my goals, and I am deeply grateful for it.

*This material is based upon work supported by the National Science Foundation under the Graduate Research Fellowship Program. Any opinions, findings, and conclusions or recommendations expressed in this publication are those of the author and do not necessarily reflect the views of the National Science Foundation.

This research has also previously been supported through the Pennsylvania Space Grant Consortium.

Chapter 1

Introduction

Small-scale multicopter aircraft are continually becoming more popular in many aspects of society, and their usefulness stretches far beyond a commercial product. The increasing demand for these aircraft comes along with an increasing need to understand how they operate so as to improve their efficiency and performance. A large set of conceptual, computational, and wind-tunnel based studies are being conducted to increase the knowledge of these aircraft. For example, Refs. 1-4 provide some studies from the NASA Ames Research Center. Prior work has also applied state-of-the-art computational analysis techniques based on computational fluid dynamics (CFD) to advanced vertical-flight aircraft design and analysis tools (Refs. 5-16).

In fact, the application of CFD to rotary-wing vehicles, which conventionally lag considerably behind their fixed-wing counterparts, is quite long. Strawn et al., Ref. 9, date the earliest rotary-wing computations as having taken place in the 1970's. The earliest computational models were of course limited by the lack of computational power available at the time. This left a lot of room for improvement considering the complexities of rotorcraft aerodynamics. Figure 1 shows one of the earliest documented accounts of the complex rotary-wing flow from Gray, Ref. 10. Over the following decades, however, advances were made and new tools implemented in line with the advances made in computing technology. The steady increase in computational power, through both improved computing hardware and better software approaches, has allowed the implementation of evermore realistic simulation approaches. The present-day capabilities tie together calculations for aerodynamic, structural, and even acoustic considerations, oftentimes providing feedback on how to optimize the vehicle's design to meet certain constraints. Figure 2 shows a simulation of the complex flow-field around a V-22 Osprey through the use of more recent

computational tools, Ref. 11. Another large area of improvement for these analysis tools has been in the accurate modeling of vehicle geometry. Figure 3 shows the detail captured in a simulation of the Apache helicopter by Aftosmis et al. Ref. 12.

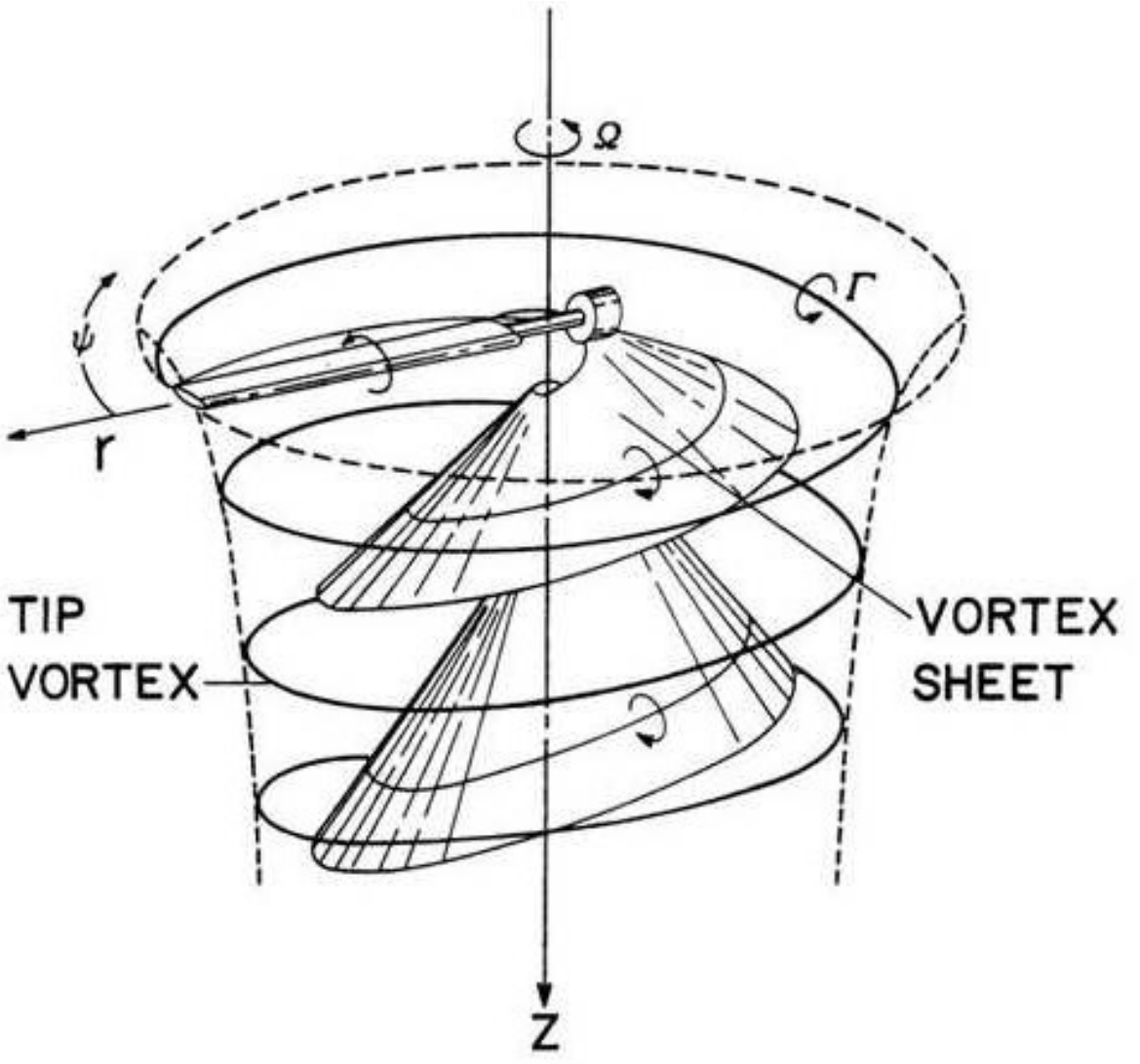

Figure 1. Complicated Flow Structure of a Rotating Wing, Gray Ref. 10

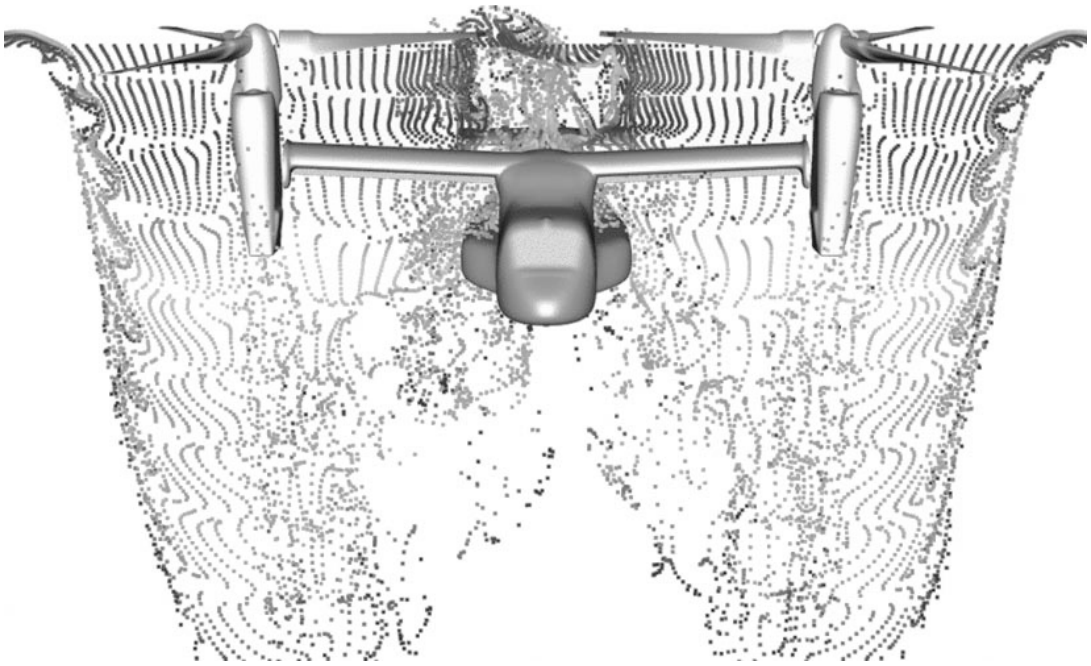

Figure 2. Flow-Field around the V-22 Osprey, Potsdam and Strawn Ref. 11

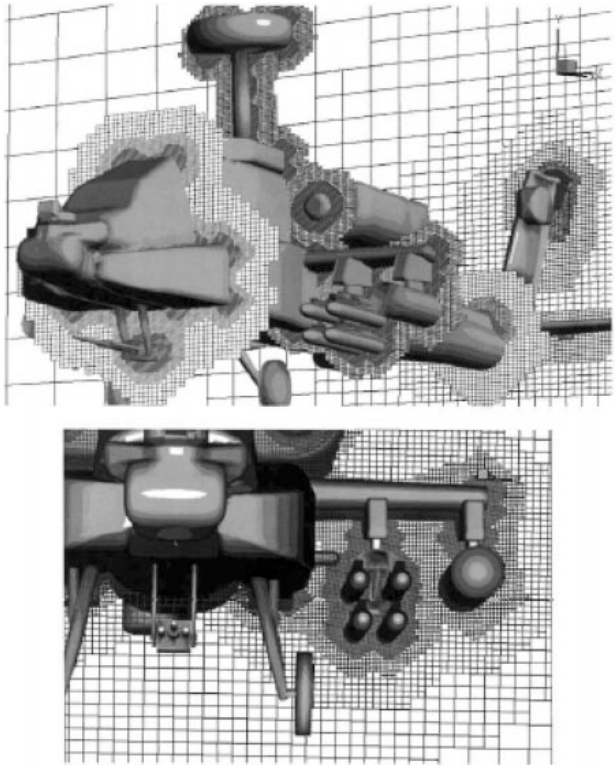

Figure 3. Computational Grid of the Apache Helicopter by Aftosmis et al. Ref. 12

Such analyses, however, have a large computational cost that is not ideal for rapid design iteration and not feasible for the average user. A high-fidelity, yet computationally less demanding, analysis tool is desired to aid in the design process of these vehicles.

In this effort, two different CFD approaches for coaxial rotor analysis are presented. The first, novel approach, is referred to as the mixing-plane approach, which is a blade-resolved method suitable for hover. This means that the boundary layer is being resolved, or calculated, over the true geometry of the rotor blades. The concept of a mixing-plane is common to turbomachinery applications, and in general is not novel. However, it does not appear to have been applied to helicopter rotors, particularly the context of coaxial rotors in hover. Some advantages of mixing-planes include: (1) smaller cell counts due to the ability to utilize periodic boundaries which nearly halve the cell count in the context of a RANS CFD model, (2) enabling the usage of steady algorithms for the rotor solution, (3) and not demanding a highly-resolved wake. In general, the approach is found to be substantially more efficient with respect to conventional methods, while retaining much of the accuracy, indicating potential computational savings for demanding hover calculations. A nearly identical "baseline" blade-resolved model was created following the conventional, or state-of-the-art, rotorcraft CFD methodology. This will be referred to as the time-accurate model, and it was created so as to observe the deviation in rotor performance calculations and computational time of the mixing-plane approach from the conventionally accepted methodology. In general, these blade-resolved models use the same computational meshes, boundary conditions, and numerical methods. The approaches differ only with the implementation of the mixing-plane interface that then allows for the use of the rotating reference frames, a steady solution approach, and periodic boundaries, thus substantially reducing the overall cell count and computational time. Although the mixing-plane model is found to agree very well with the

conventional time-accurate model in hover and has a run time that is more than two orders of magnitude less, the current physics modeling breaks down when applied to edge-wise rotor flight conditions such as forward flight. Since a highly efficient coaxial rotor model was also desired for use in forward flight, a second modeling approach was needed.

The second approach presented in this work is blade-modeled, meaning that the influence of the blades is represented by means other than a true resolving of the boundary layer on them (i.e. blade-resolved). This approach adds the capability to analyze multicopter configurations in forward flight, and can also be used in hover, axial climb, and axial descent. The specific modeling approach incorporates a blade-element model to represent the rotors. This modeled description of the rotor then operates within a CFD resolved domain, maintaining a level of fidelity through the proper capturing of the rotor inflow and wake. The blade-modeled approach is developed in parallel between two different CFD programs, STAR-CCM+ (Ref. 17) and RotCFD (Ref. 18), so as to compare the results from two independent solution methods. Comparison to a high-fidelity blade-resolved simulation shows that this blade-element model has sufficient accuracy with an even further reduction in computational requirement as compared to the mixing-plane model. This blade-modeled approach also allows for coaxial rotor analysis in various flight conditions such as forward flight, hover, axial climb, and axial descent.

The following sections will give a more in-depth explanation of these modeling approaches, the objectives of this research, a brief summary of CFD development up to the current state-of-the-art multicopter analyses, and a summary of the CFD programs and computational resources used in this work. Chapters 2 and 3 then step through the development of the blade-resolved and blade-modeled approaches, respectively. In Chapter 4, results for the blade-resolved approach, and then the blade-modeled approach, are presented along with further analyses of a

coaxial rotor system. Lastly, conclusions and future work are discussed in Chapter 5.

Rotorcraft Analysis Methods

Various methods have been developed to analyze the aerodynamic performance of rotorcraft, while balancing the fidelity of the solution with computational cost. On one end of the spectrum are those methods that model the blades, which have simplifying assumptions enabling fast simulations. Examples of blade-modeled approaches are blade-element momentum theory, free-vortex wake, and actuator-disk methods. These approaches are good for a preliminary design in many cases; however, if the airfoil characteristics are unknown, or in complex interactions, they may not be well suited to the analysis needed for a final design. On the other end of the spectrum are blade-resolved approaches, which include blade-resolving CFD methods such as Reynolds-averaged Navier-Stokes (RANS), detached-eddy simulation, and large-eddy simulation. These approaches are referred to as blade-resolved because they aim to directly solve a modeled form of the Navier-Stokes equations around a resolved rotor blade. These high-fidelity models directly account for the blade shape and accurately compute the rotor's influence at a much higher computational cost, which in some cases can have a solution time of several months.

Recently, these high-fidelity CFD approaches have been used for the analysis of unmanned aerial systems (UAS), and of particular interest here is their application to multicopter UAS. The NASA code OVERFLOW, for example, has recently been used heavily by the NASA Advanced Supercomputing Division (NAS) to analyze commercially available UAS such as the DJI Phantom 3. Figures 4-5 show an image of the aircraft's computational grid in OVERFLOW, and a flow solution of Q-criterion highlighting the highly intricate wake structure around and beneath a multicopter vehicle, Ref. 8.

Figure 4. Computational Grid of DJI Phantom 3, Yoon et al., Ref 8

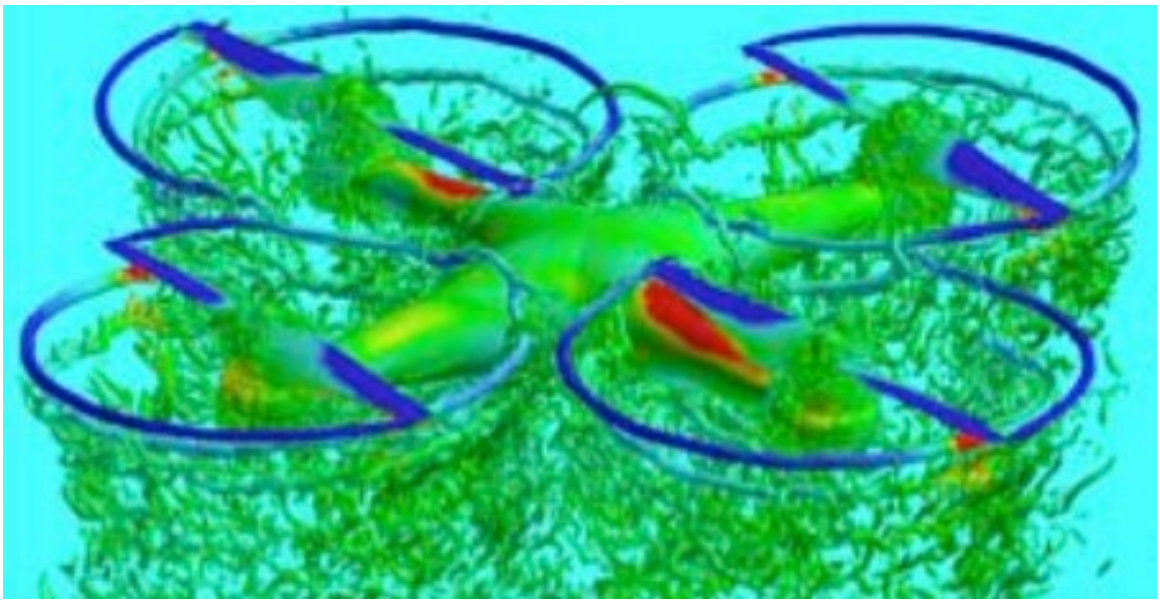

Figure 5. Flow Solution of DJI Phantom 3 Showing Complex Wake Structure, Yoon et al. Ref. 8

These simulations are rapidly growing in complexity to match the already developed CFD capabilities. The simulation of the DJI Phantom 3 by Yoon et al., Ref 8, incorporates 74 overset grids with about 225 million cells to account for the motion of all four rotors and the fuselage interaction. The simulation solves the compressible Navier-Stokes equations using a delayed detached eddy simulation approach with an SA turbulence closure for the RANS equations. This simulation setup requires a run time on the order of 2-3 days on 1024 computational cores of the NAS supercomputer, Pleiades. It should be evident, that this simulation is not feasible for the average user. This highlights the main issues with the current state-of-the-art approaches to multicopter UAS analysis with CFD, which are computational time and resources. This thesis will work to address these issues. Figure 6 shows a comparison of the computational requirement versus model fidelity for the various methods.

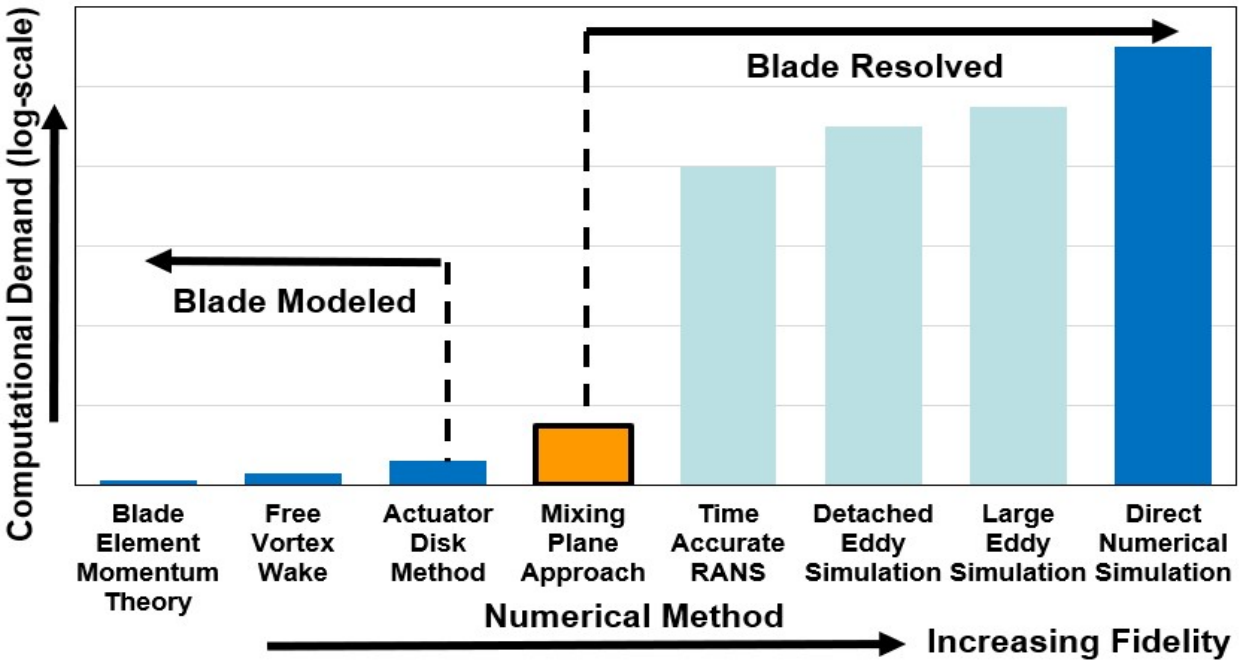

Figure 6. Comparison of Computational Time vs. Model Fidelity for Various Computational Approaches Applied to Coaxial Rotors

CFD Software and Computational Resources

The commercial CFD toolsets, STAR-CCM+ and RotCFD, are used in this work. Both software packages contain provisions for the entire workflow, starting from creating the baseline geometry all the way through visualizing the results. In the context of this research, STAR-CCM+ was used to create both a blade-resolved analysis that properly resolves the boundary layer on the three-dimensional rotor geometry, and a blade-modeled approach that represents the rotor with a line of momentum sources, which impart momentum into the flow based on the local CFD resolved inflow and the specified airfoil performance look-up tables. The RotCFD toolset incorporates a similar blade-modeled approach to that described for STAR-CCM+. The technical details of the simulations and their modeling methods are presented in their respective sections.

The computational resources used in this research were the Penn State Aerospace Engineering Department's computing clusters. The computing clusters used range in size from 432 to 1,536 physical cores. The number of physical cores for any particular job was chosen to get close to 100,000 cells per core, which was found to provide the most time-efficient balance between computation time per core and communication time between them. The required computational time for each model is defined as the number of cores used multiplied by the wall time. Computing clusters provided a large benefit for STAR-CCM+ calculations through MPI-based parallelization. However, RotCFD can only be run using open-MP or open-CL (GPU-accelerated). Hence, using RotCFD on a workstation (quad-core processor, 32 GB of RAM, and a Nvidia GeForce GTX 1060 graphics card with 6 GB of VRAM) performed substantially better with the graphics card than on the clusters. The large number of nodes available on the clusters used, however, eventually overtakes the capability of running one GPU-accelerated case at a time with the open-CL framework. The addition of GPU nodes to a cluster could greatly enhance the

computational capability. Rajagopalan et al. (Ref. 19) documented the computational benefits observed by exploiting this technology for CFD applications in the RotCFD toolset.

Thesis Objectives

The present research effort involves expanding the tools for analysis of multicopter aircraft through studying two separate CFD approaches. The first approach presents a novel and efficient methodology that retains a high-fidelity, three-dimensional, blade-resolved CFD evaluation of a hovering rotorcraft. The research to date has not yet addressed the issues that arise in applying this approach to forward flight. Therefore, a second computational approach, using a blade-element method, was explored to efficiently simulate this flight regime for multicopter vehicles. The model is found to yield even further savings in computational time and effort, allowing for coaxial rotor solutions in two hours on a workstation with a GPU, while still maintaining the accuracy associated with properly modeling the rotor inflows and wakes. This second modeling approach is applied to the same coaxial rotor system that was used in the development of the computational models. The rotor system is analyzed in hover, axial climb, forward flight, and motor-out conditions. These objectives are summarized below.

The objectives of this thesis are to:

1. Develop an efficient blade-resolved approach for multicopter analysis in hover.
2. Create a blade-modeled approach for analysis of multicopter rotors in various flight conditions.
3. Use the blade-modeled approach to analyze a coaxial rotor configuration.

Chapter 2

Blade-Resolved Approach: STAR-CCM+ Mixing-Plane Model

The first portion of this research incorporates a blade-resolved RANS CFD approach using a technology referred to as a mixing-plane. The approach retains many of the benefits of blade-resolved methods but implements assumptions that allow for a large reduction in computational time. The model approach is still able to capture all the relevant aspects of the rotor system, i.e., the loss of lift from the blade tip vortex, hub effects, rotor inflow, and refined wake regions to resolve the rotor-rotor interaction and rotor wake.

This chapter describes the progression of this CFD tool from the initial two-dimensional model to the final blade-resolved mixing-plane rotor model. Each model discussed adds additional features and complexity to the simulation. The CFD model is first evaluated and benchmarked using aerodynamic predictions for an airfoil, a semi-span wing, and a rotor blade. The airfoil model used by both blade-resolved simulations is presented in the next section. In this step, a two-dimensional model was created for the NACA 23012 airfoil. Following grid studies of the airfoil model, the non-rotating model was developed. This created the three-dimensional grid that is then applied to the coaxial rotor. At this point, the model is extended to hover conditions with the mixing-plane approach for single and coaxial rotor systems. Additionally, the same condition is also evaluated using the conventional time-accurate model, meaning that it has grid motion and temporal resolution in line with the current state-of-the-art. Figure 7 shows a road-map of the blade-resolved model progression.

Comparing results between the mixing-plane approach and the time-accurate model, in Chapter 4, characterizes the mixing-plane method with respect to accuracy and computational time. The results indicate that the present approach has significant computational savings at a small

cost to accuracy, which is better suited for design purposes in hover conditions.

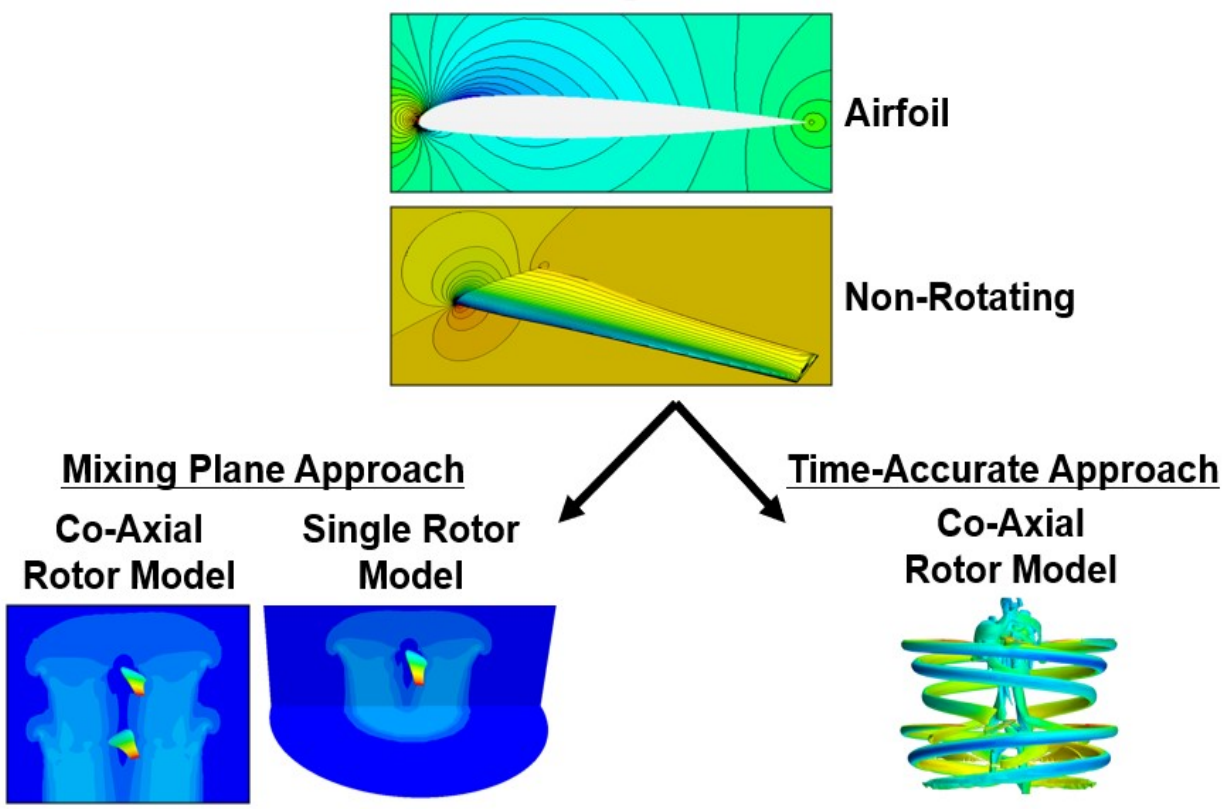

Figure 7. Blade-Resolved Approach: Progression of Mixing-Plane and Time-Accurate Model Development

Airfoil Model

The first step in creating this analysis tool was to develop the grid around a two-dimensional airfoil. This portion of the research used the NACA 23012 airfoil. The model incorporates a C-type grid around the airfoil that is overset with the background domain. The overset boundary allows the angle-of-attack (AOA) to be changed without having to regenerate the grid. The domain boundaries are at twenty-five chord lengths. Figures 8-9 show the near-body grid around the airfoil and the overset boundary, respectively.

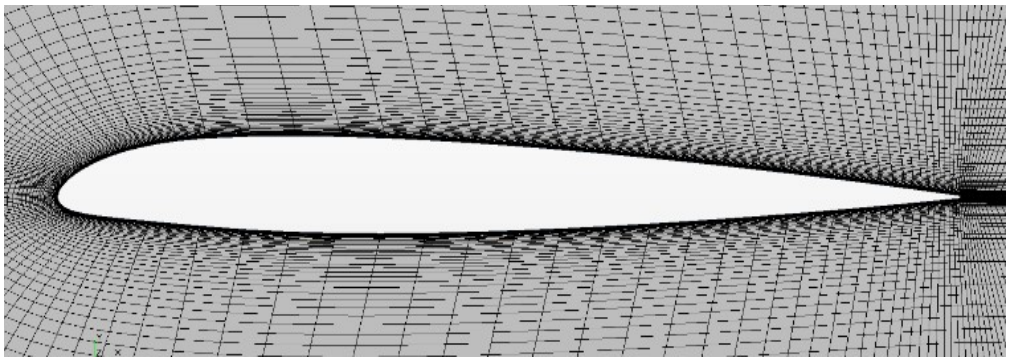

Figure 8. Airfoil Model C-Type Grid (NACA 23012)

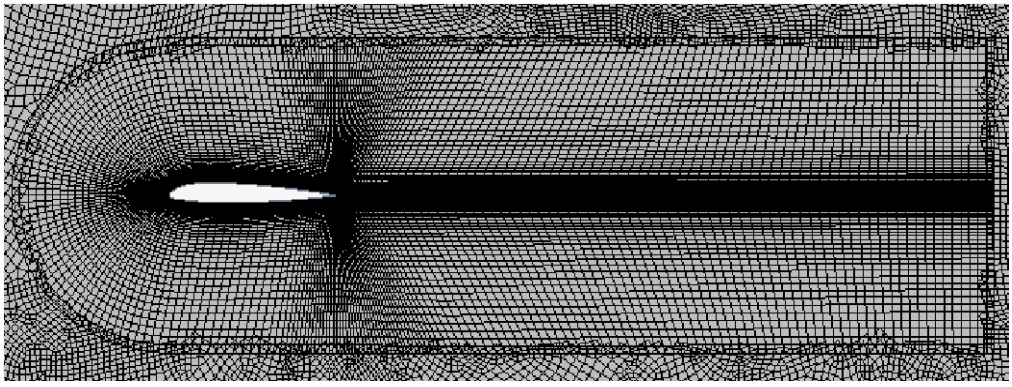

Figure 9. Airfoil Model Overset Grid (NACA 23012)

A grid resolution study (GRS) was conducted to verify the airfoil model. The goal of the optimization was to reduce the overall cell count, while maintaining an acceptable fidelity. This is done to keep the final cell count in the three-dimensional models at a manageable number, which was below 35 million in the present research. The model incorporates a quadrilateral unstructured mesh for the background with a volume constraint around where the overset body is located. This forces a 1:1 cell aspect ratio at the overset boundary. The C-type grid was generated using the STAR-CCM+ directed mesh tool, which allows for precise control of a structured near-body mesh. The final C-type mesh extends five chord lengths downstream of the airfoil and incorporates 131 wrap-around points along the airfoil contour, a trailing edge (TE) chordwise spacing matching the

TE thickness of 0.23% of the chord length, a leading edge chordwise spacing of 0.20% of the chord length, and a 15% maximum growth rate on connected cells. A first cell size was selected to give a y+ equal to 45 based on a chord Reynolds number of $3x10^6$. The STAR-CCM+ All-y+ wall treatment, a hybrid model rooted in wall functions that adjusts based on the local y+, is used in the model. A RANS solver with Spalart-Allmaras (SA), Ref. 20, turbulence closure was used for the simulation. In addition, a SIMPLE-based segregated solution method is used for the numerical model (Ref. 21). Figure 10 shows pressure contours for the airfoil model at zero AOA.

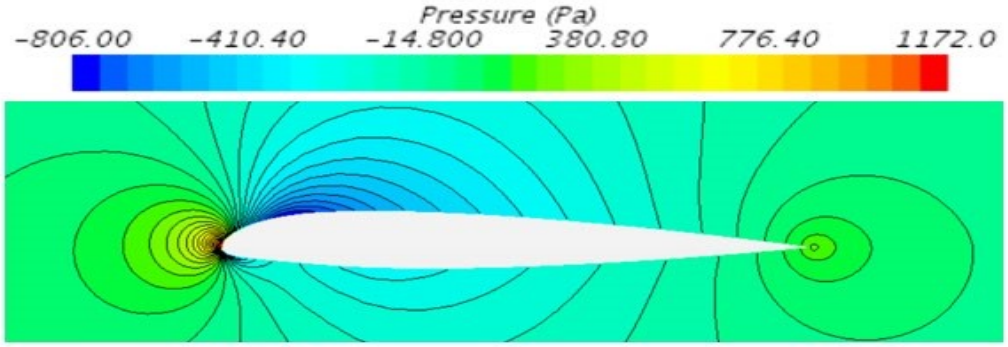

Figure 10. Airfoil Model Pressure Contours (NACA 23012, Re=$3x10^6$, Ma = 0.2, AOA = 0)

A comparison was carried out with results obtained from XFOIL, Ref. 22. XFOIL is a panel method solver that is coupled to a two-equation, integral-boundary-layer solver to account for viscous effects. A densely populated XY coordinate table of the NACA 23012 airfoil was generated using the XFOIL paneling feature. The airfoil was then analyzed at the same Reynolds number of $3x10^6$ and Mach number of 0.2 with forced transition at the leading edge to simulate the fully-turbulent flow in the CFD model. Figure 11 shows the XFOIL graphical user interface with the airfoil, its pressure distribution, and the airfoil's performance coefficients for an angle-of-attack of 5 degrees.

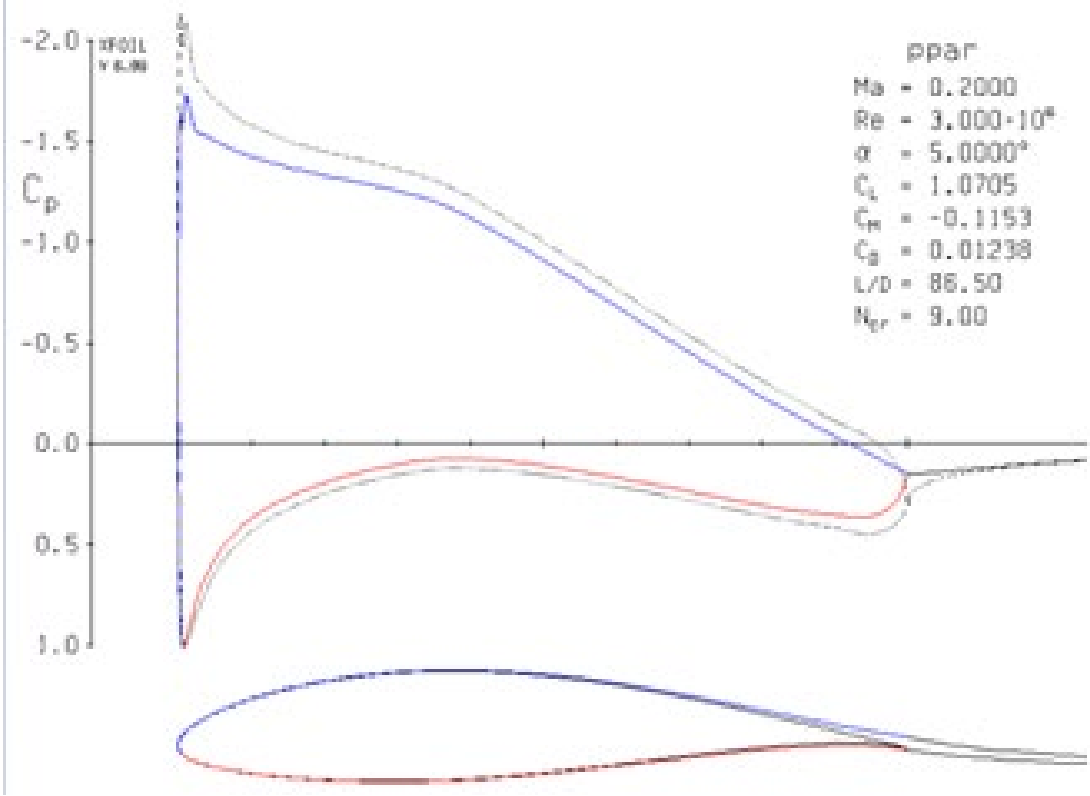

Figure 11. MIT-XFOIL Airfoil Analysis Code (Ref. 22)

Figure 12 shows a comparison of the surface pressure coefficient around the airfoil at zero AOA for both XFOIL and STAR-CCM+. The pressure coefficient matches along the entire chord length, and only a slight deviation is observed at the TE. Values of lift coefficient, drag coefficient, and lift-to-drag versus angle of attack were gathered from both XFOIL and the STAR-CCM+ model. Comparing results obtained in Figure 13 shows good agreement between the two methods. The lift and drag predictions deviated by a maximum of 1% and 8%, respectively. These values also agreed with experimental data in Abbott and Von Doenhoff (Ref. 23). The strong correlation provided sufficient confidence in the model's ability to accurately predict attached boundary layer flows where XFOIL is known to perform well. A model with higher refinement had been even closer to the XFOIL drag predictions, but the current deviation was deemed acceptable in order to maintain a reasonable cell count.

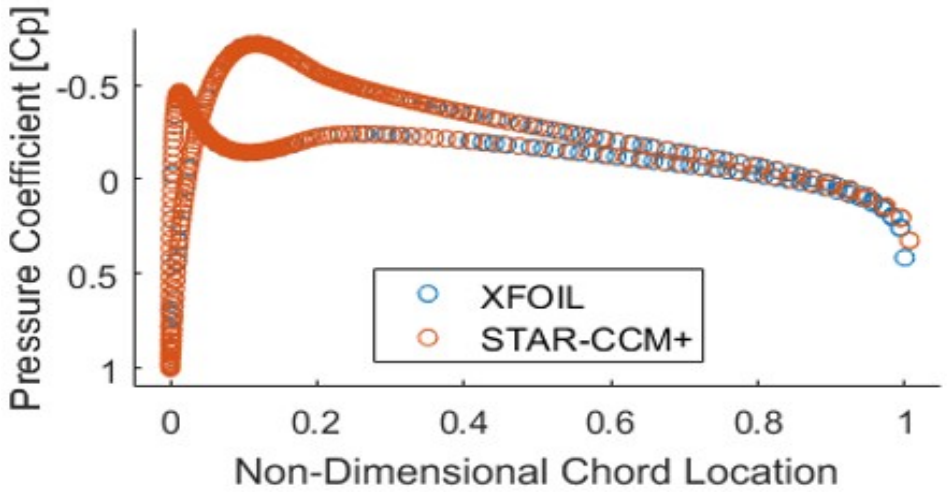

Figure 12. Pressure Distribution Comparison of Airfoil Model and XFOIL (NACA 23012, Re=3x10^6, Ma = 0.2, AOA = 0 deg.)

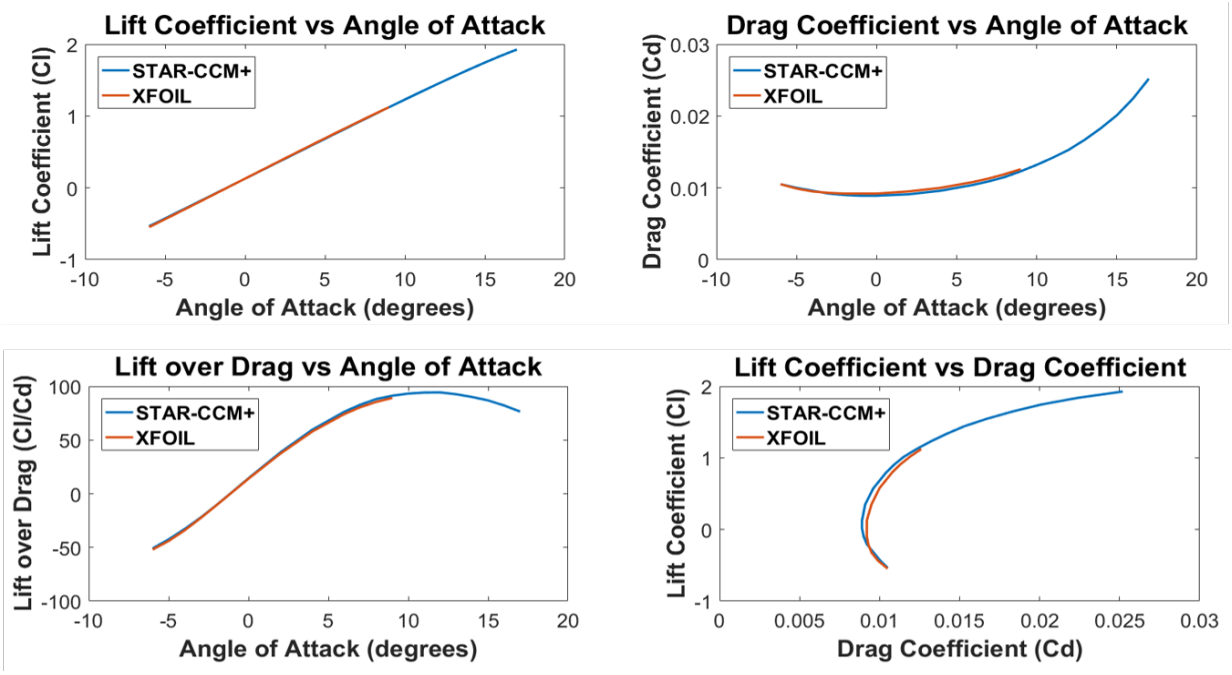

Figure 13. Airfoil Model Comparison with XFOIL (NACA 23012, Re = 3x10^6, Ma = 0.2)

The purpose of the non-rotating model was to implement the grid of the optimized two-dimensional airfoil into a three-dimensional model. A twist and taper distribution were used to create a full blade. Then the grid was generated through extrapolating the C-type mesh along the

span of the blade; this was done using the directed mesh tool within STAR-CCM+ to obtain a structured three-dimensional mesh on the blade. The model was set up so as to allow for a comparison with PSU-XTurb, Ref. 24, which was used to run a lifting-line theory simulation. This was done by imposing a symmetry plane along the maximum chord to simulate a semi-span wing.

A process similar to the extrapolation of the C-type mesh was used for the background and overset regions. Blade tip refinement methodology was also developed to capture the blade tip vortices. The cell size along the span of the blade was adjusted to provide a blade tip first-cell width close to the first cell height. This size was used for the blade tip volume control, and it was then subsequently increased in the off-body region to provide a 1:1 cell volume ratio with the background region at the overset boundary. The simulation uses RANS with SA turbulence closure chosen to accurately model the steady, attached flow. The comparison with PSU-XTurb found the lift to match within 1.5%. Figures 14-15 show the non-rotating model grid and pressure contours, respectively.

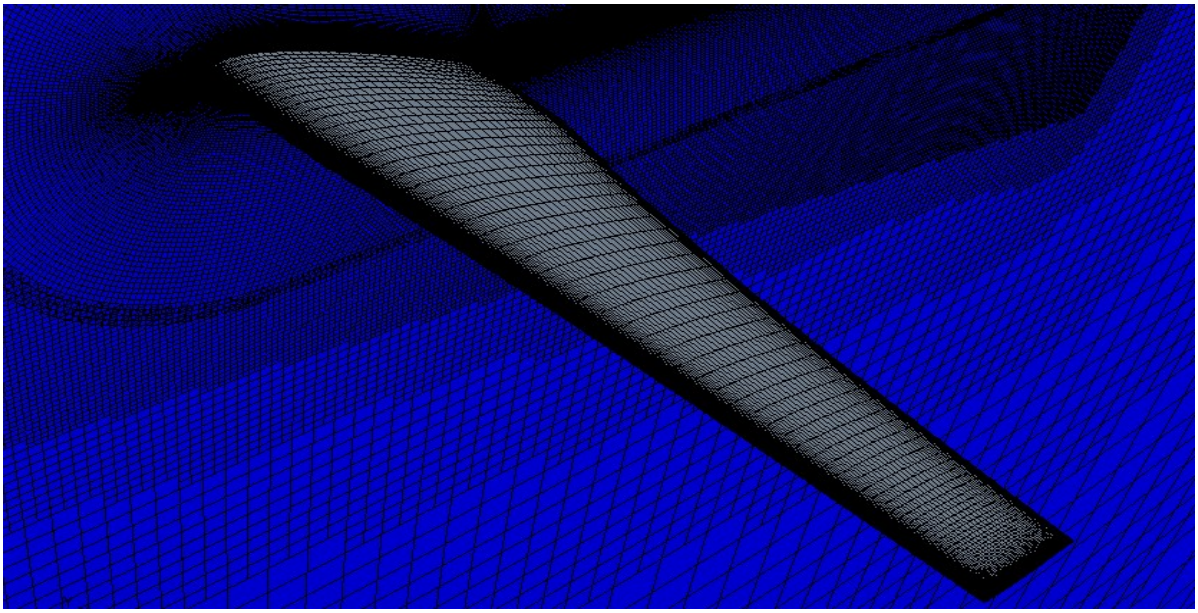

Figure 14. Non-Rotating Model – Grid (Modified Blade Planform)

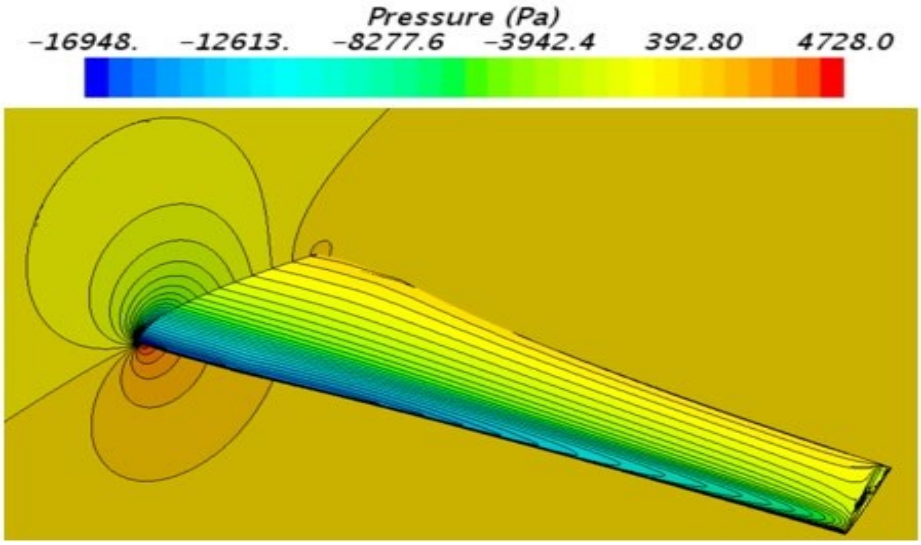

Figure 15. Non-Rotating Model – Pressure Contours (Modified Blade Planform)
Mixing-Plane Approach

The next model incorporates the mixing-plane boundary type, which is common to turbomachinery applications. The boundary is split into concentric rings, or bins, and the flow passing through the boundary is averaged on each individual bin. This provides a circumferentially averaged flow solution at the mixing-plane interface.

This proposed CFD approach provides three substantial benefits. The model approach allows for (1) the solution in a rotating reference frame, (2) the use of periodic boundaries to reduce grid size, and (3) averaging of the rotor wake at a location sufficiently below the rotor thus reducing the demand for high wake refinement. The periodic boundary, which requires only one blade per rotor to be modeled regardless of the number of blades on the rotor, provides a significant reduction in the total cell count. This is because the blades are one of the regions demanding the most computational cells. The ability to use a rotating reference frame is another time-saving aspect of the present research. This is because the solution becomes a steady solution method, eliminating the need for grid motion and temporal resolution. It will be shown that eliminating the time-accurate aspect of the model is what dominates the computational savings in the present model.

Lastly, the present model also alleviates the computational requirements for the rotor wake. For hover, these are quite significant. The present approach eliminates the need to resolve a wake dominated by tip vortices far below the rotor since the mixing-plane averages these vortices, and the resulting wake becomes favorable to a coarse rotor-wake mesh, while retaining the rotor inflow distribution to acceptable accuracy for preliminary design.

Figure 16 shows an example of the mixing-plane boundary in a turbomachinery application. One blade on both the rotor and the stator are outlined with a periodic boundary, signifying that they are the only blade of each respective stage being modeled. The mixing-plane boundary can be seen coming straight down the middle of the diagram.

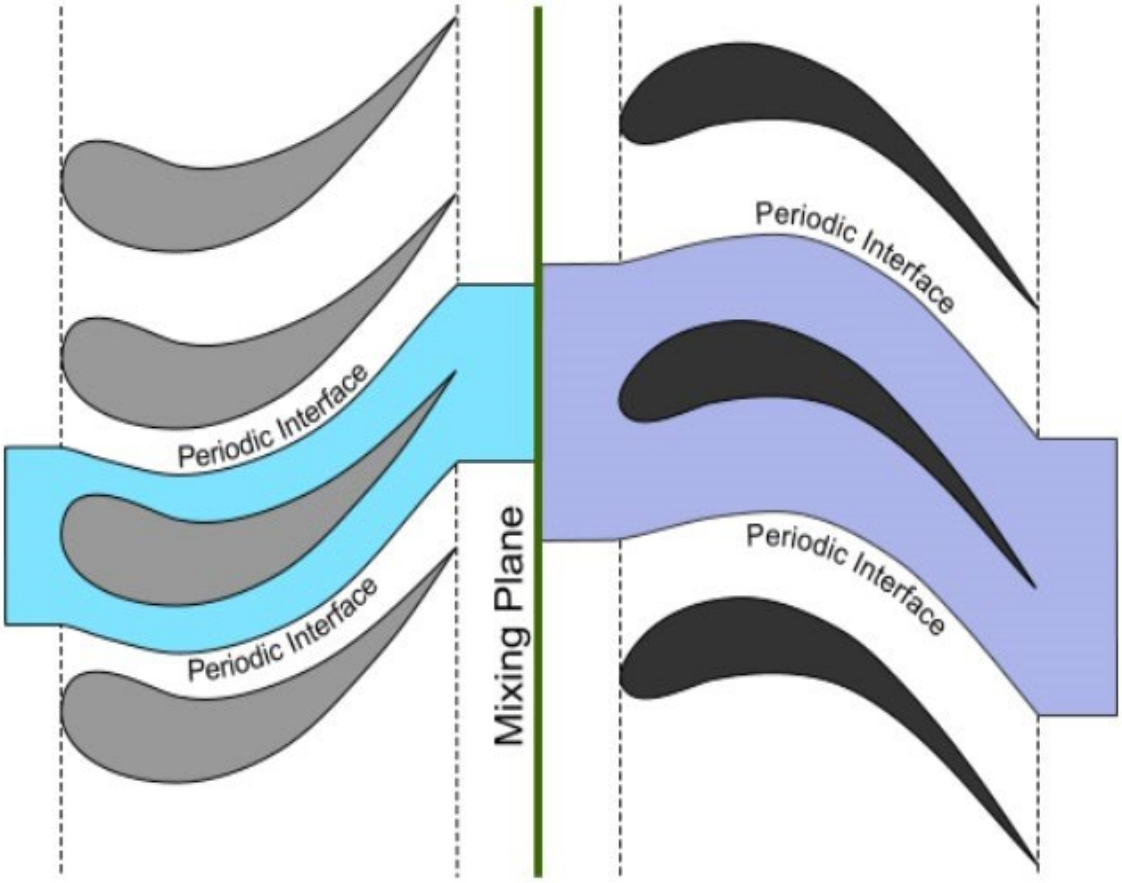

Figure 16. Illustration of Mixing-Plane Approach (Ref. 17)

Mixing-Plane Single Rotor Model

This first mixing-plane model added in the complexities of a rotating reference frame, the mixing-plane boundaries, wake refinement, and a periodic boundary. The modeled coaxial rotor has two blades per rotor, which means that only one of the two blades is physically included in the grid for the single rotor model as can be seen in Figure 17. The white space in the image represents a void region, half of the cylindrical disk, where there are no grid cells. The periodic boundary maps the flow solution from the modeled blade onto the other half of the region. The bold black lines on the image represent the mixing-plane boundary interface. Figure 18 shows another image of the grid including the blade, periodic boundary, and the lower mixing-plane boundary. Figure 19 shows velocity contours for the mixing-plane single rotor model. The blade tip vortices, contraction of the wake, and root cut-out effects can all be observed.

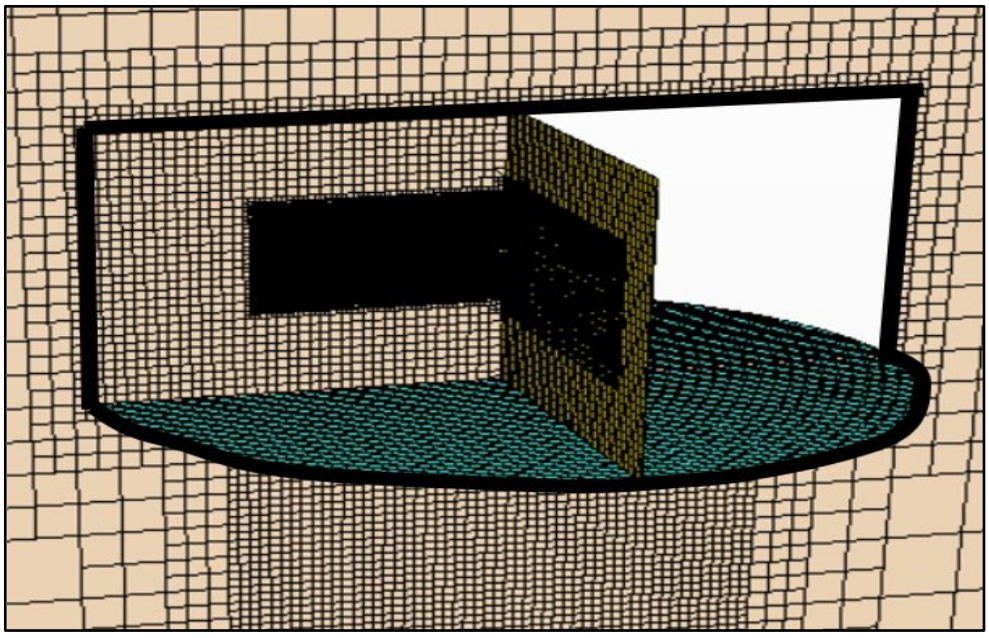

Figure 17. Mixing-Plane Single Rotor Model – Grid
(Mixing-Plane Boundaries Outlined in Black)

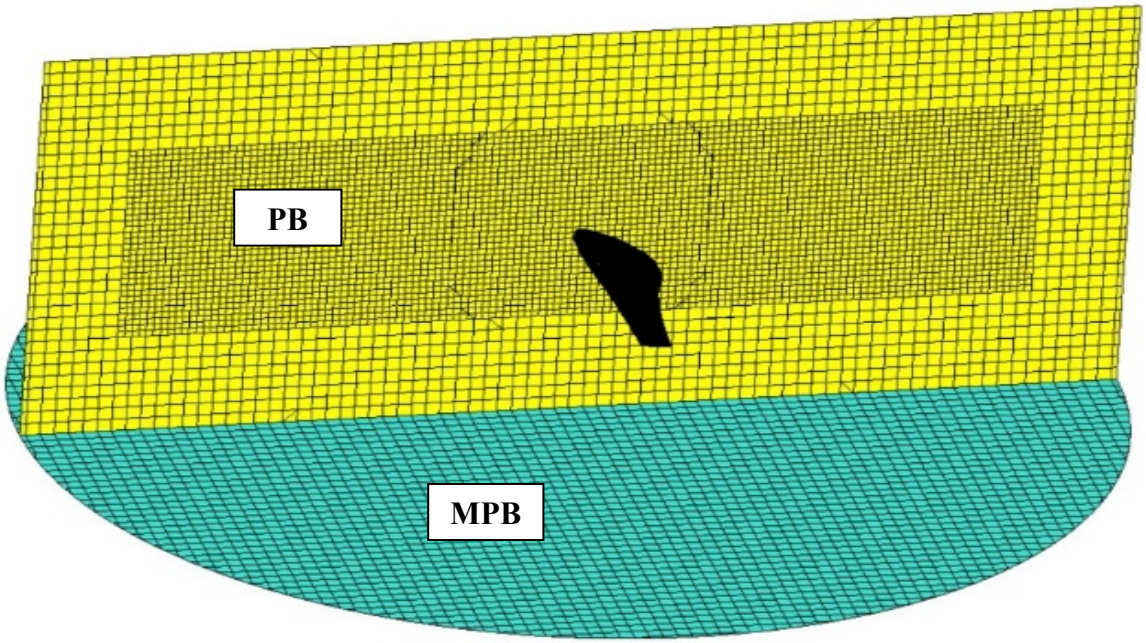

Figure 18. Mixing-Plane Single Rotor Model – Periodic Boundary (PB)

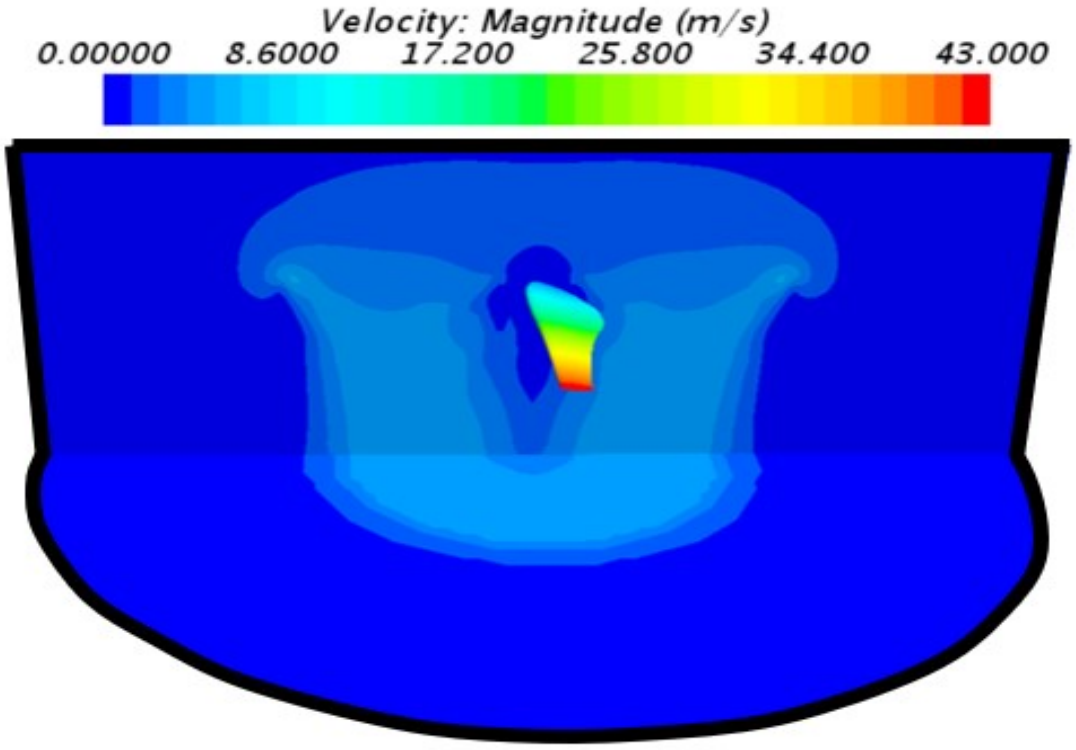

Figure 19. Mixing-Plane Single Rotor Model - Velocity Contours on Periodic Boundary and Lower Mixing- Plane (Mixing-Plane Boundaries Outlined in Black)

Mixing-Plane Coaxial Rotor Model

The mixing-plane coaxial rotor model uses the same set up developed for the single rotor model with the second rotor added 0.4 rotor diameters below the first one. The single rotor model had a coarsened grid, since its purpose was only to develop the methodology. This coaxial model re-introduced the refined grid parameters that had been found through the airfoil model and subsequent grid resolution studies. Further grid resolution studies were carried out on this model to determine the required refinement around the blade tips and in the rotor wake. The model uses counterrotating reference frames with the mixing-plane in-between them. Figure 20 shows the outlined mixing-plane boundaries. Figure 21 shows the velocity contours around the blades and in the wake. The lower rotor can be seen as operating in the fully-developed contracted wake of the upper rotor. Figure 22 shows pressure contours at the blade tip.

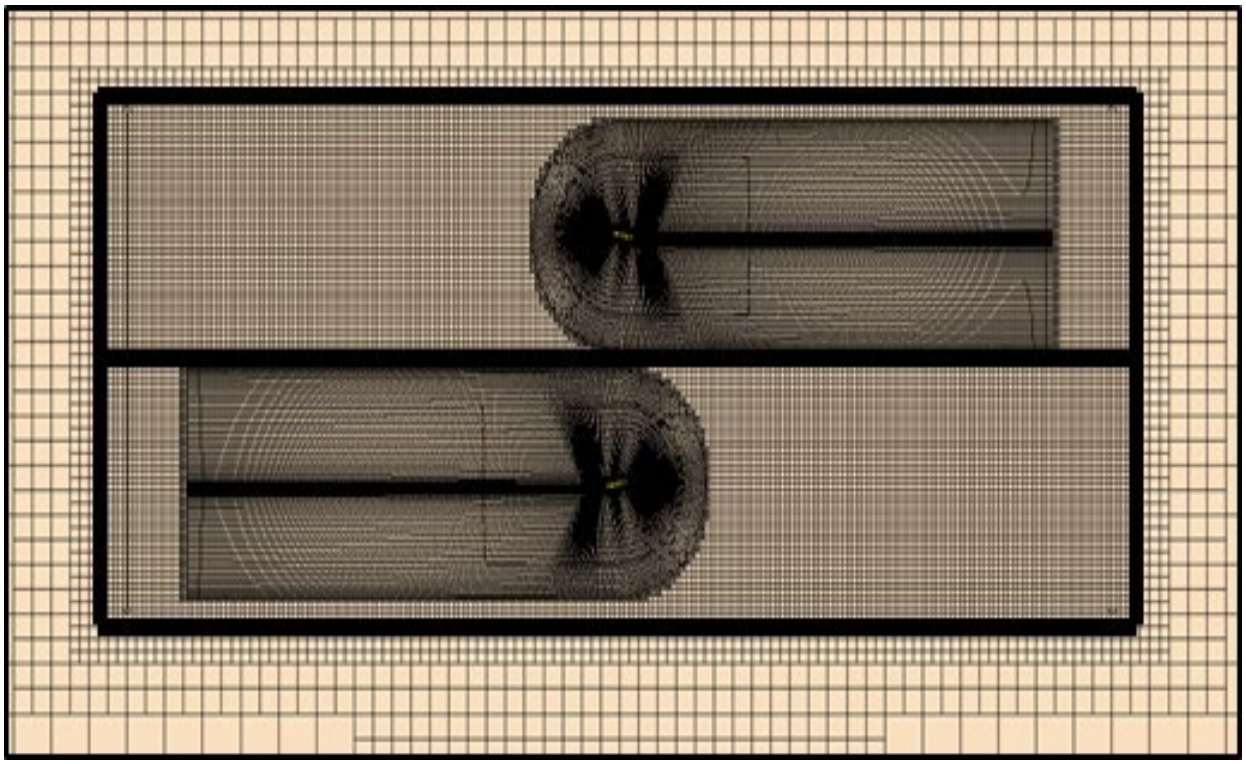

Figure 20. Mixing-Plane Coaxial Rotor Model – Grid
(Mixing-Plane Boundaries Outlined in Black)

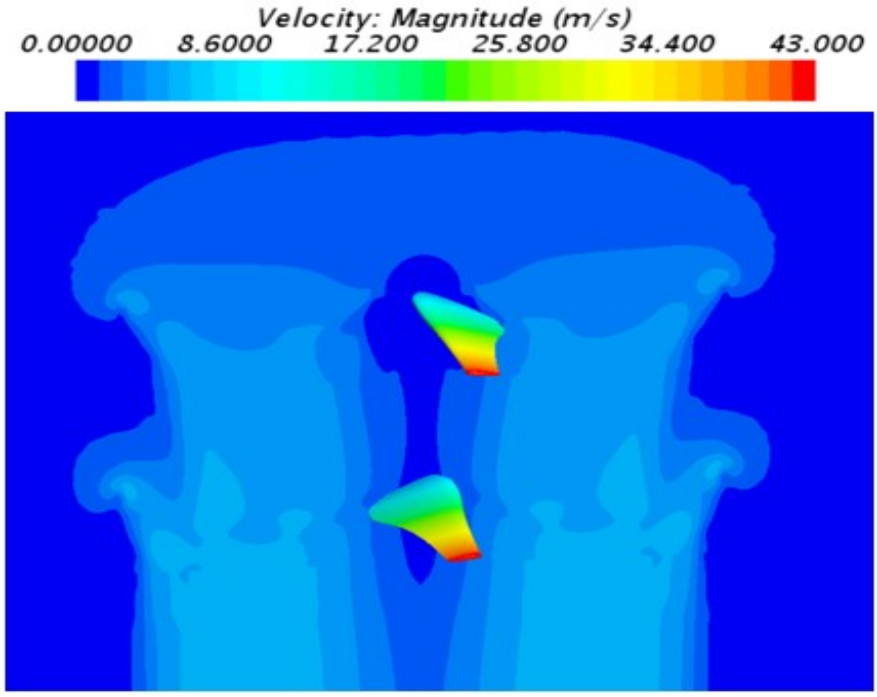

Figure 21. Mixing-Plane Coaxial Rotor Model - Velocity Contours on Periodic Boundary

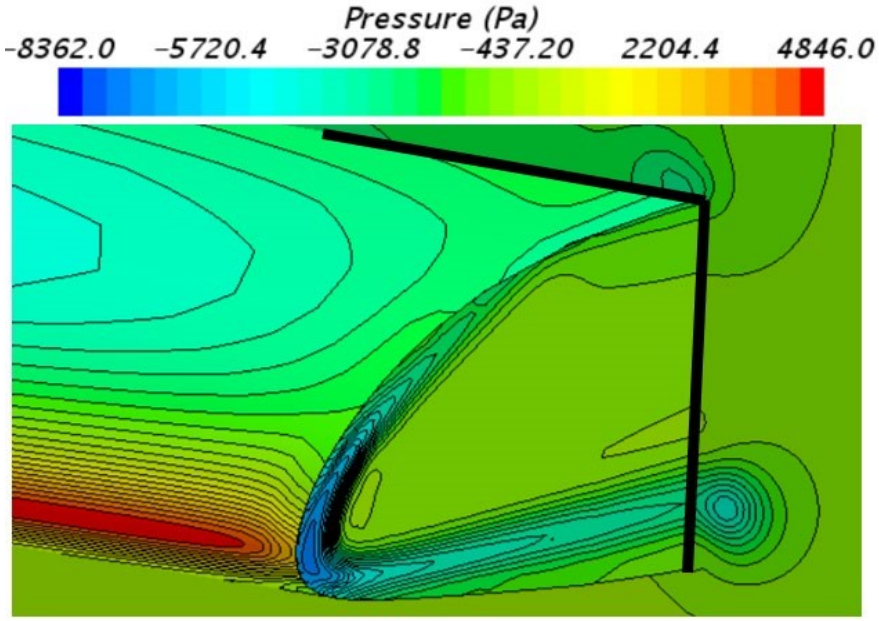

Figure 22. Mixing-Plane Coaxial Rotor Model - Pressure Contours on Blade and Spanwise Cut-plane (Cut-plane Boundary Outlined in Black)

Time-Accurate Coaxial Rotor Model

In order to compare the proposed mixing-plane approach to conventional best practices, a time-accurate coaxial rotor simulation was run. The grids are identical between the two models, and the time-accurate model includes the two additional blades that were removed from the mixing-plane model with the use of periodic boundaries. The final model has 31.9 million cells, roughly twice as many as the mixing-plane model. Instead of mixing-planes, sliding-grid interfaces are used within an unsteady time-accurate URANS solver using an SA turbulence model. The model was run with two different physical time-step sizes of 1.5 degrees and 0.25 degrees that will be referred to as the coarse and refined runs, respectively. Each time step had 20 sub-iterations in order to decrease the residuals by at least two orders-of-magnitude per time step. Figure 23 shows a cross-section of the grid through all four blades and their C-type meshes. Figure 24 shows an isosurface of two rotor revolutions with a Q-criterion of 500 colored by the local velocity, which shows the blade tip vortices being cleanly captured, convected downward, and contracting.

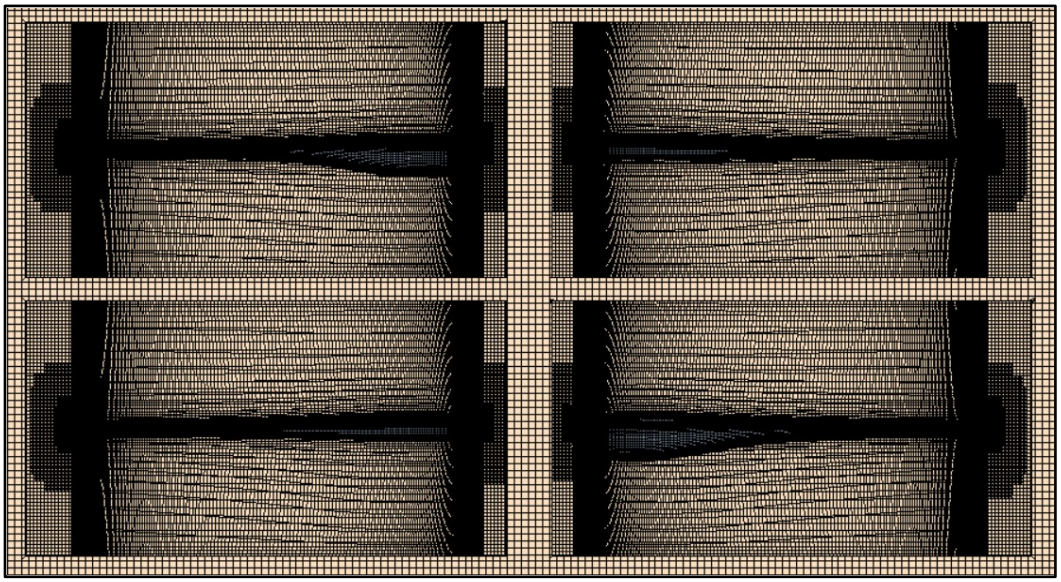

Figure 23. Time-Accurate Coaxial Rotor Model – Grid (Four Blades with C-type Grids Shown)

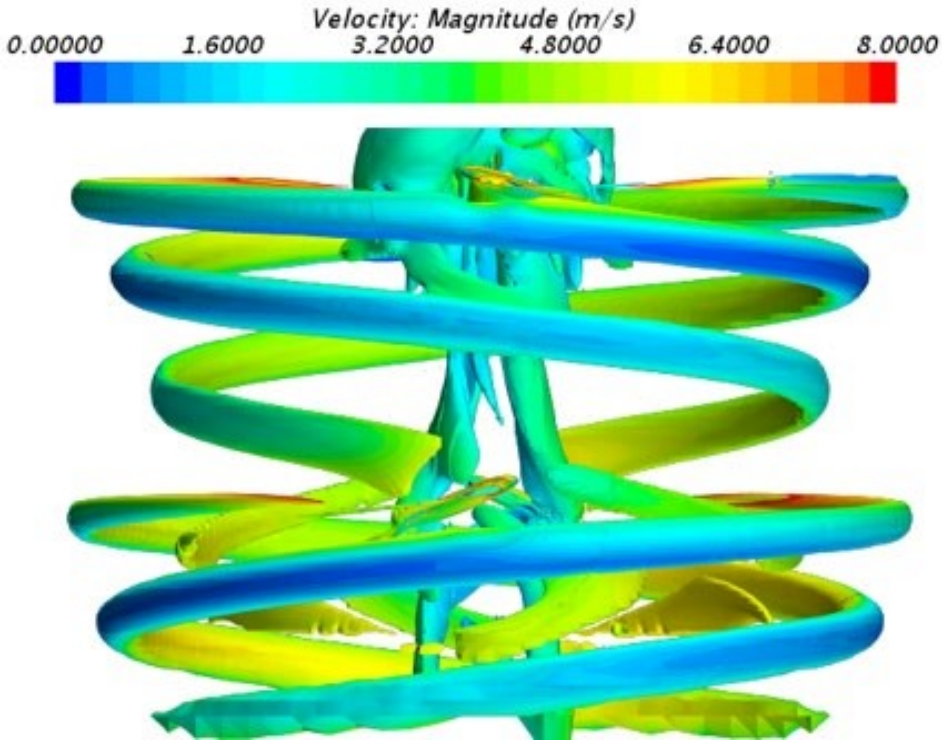

Figure 24. Time-Accurate Coaxial Isosurface – Q-Criterion = 500 [1/s^2]
Flow After 2 Revolutions Shown

The results comparing the novel mixing-plane approach with the conventional time-accurate approach are discussed first in a combined section, Chapter 3, for all results of the present research. Before that, however, development of the second model type, which uses the blade-element model approach as discussed previously, is presented.

Chapter 3

Blade Modeled Approach: STAR-CCM+ & RotCFD Blade-Element Models

The chapter discusses a blade-modeled CFD approach in the form of a blade-element model in both the STAR-CCM+ and RotCFD programs. This second set of models was developed in an effort to better capture the true coaxial rotor performance in forward flight conditions. This approach uses look-up tables for the airfoil performance in conjunction with a CFD resolved inflow to locally impart momentum into the flow, thus representing the influence of the rotor. The blade-element model presented combines the computational savings of the blade-modeled approach with the improved accuracy, as compared to lower-order methods, of a time-accurate RANS solution method in the domain to correctly capture the inflow, rotor-rotor interaction, and wake. This allows for proper modeling of the loss-of-lift at the blade tips and the loss-of-lift on the lower rotor due to its operation in the downwash of the upper rotor. The final model's potential capabilities will also be discussed.

First is the generation of the airfoil deck using MIT-XFOIL and C81 Generator, which is a wrapper for ARC2D (Ref. 25). The details of these analysis tools are discussed when they are implemented in their respective sections. A single rotor model was developed first in each program, followed by the full coaxial rotor model. Figure 25 shows a road-map for the progression of the blade-modeled approach. A comparison of the two models is discussed in Chapter 4.

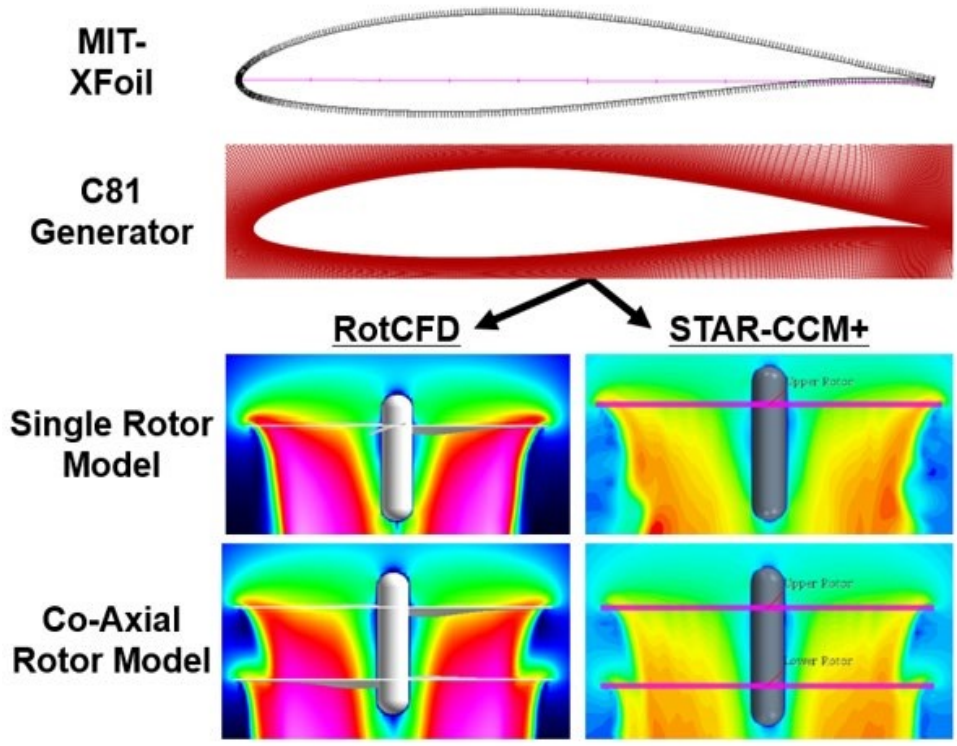

Figure 25. Blade-Modeled Approach: Progression of Blade-Element Method Model Development in RotCFD and STAR-CCM+

Airfoil Deck Creation

This sub-section details the generation of the airfoil deck used in the blade-element models. The airfoil deck, which includes lift coefficient, drag coefficient, and moment coefficient for the angle-of-attack range was first generated using XFOIL in the same manner as discussed in the airfoil model sub-section.

The same study was then conducted using the higher-order analysis C81 Generator tool. This program provides a user-friendly GUI for the ARC2D CFD program. The program uses the two-dimensional thin-layer Navier-Stokes solver with a structured airfoil fitted grid. The user inputs Reynolds number, Mach number, and specifies the angle-of-attack range for the solver. The authors decided to use a blunt TE with an O-grid, since this was believed to best simulate a

production airfoil. The TE thickness was held constant for the last 2.5% of the chord, which gave a thickness close to 0.25% of the chord, and it also followed the original camber line. Figure 26 shows the airfoil grid, including a far-field view, airfoil view, and TE view. A GRS, following the approach used by Koning et al. (Ref. 26), was conducted to determine the appropriate grid density and airfoil TE geometry. The approach uses a y+ value of 0.5, calculated using the design Mach number of 0.2. The cell-density is then increased from the program's baseline case, Grid 1, while keeping the ratio of periodic cells to normal cells constant. Once the average deviation from one refinement level to the next was less than 1%, the grid was determined to be sufficiently refined. This gave a drag deviation from the previous grid that was within one drag count throughout the linear range, which is the accuracy of the C81 Generator program's output. Table 1 shows the grid parameters from the GRS.

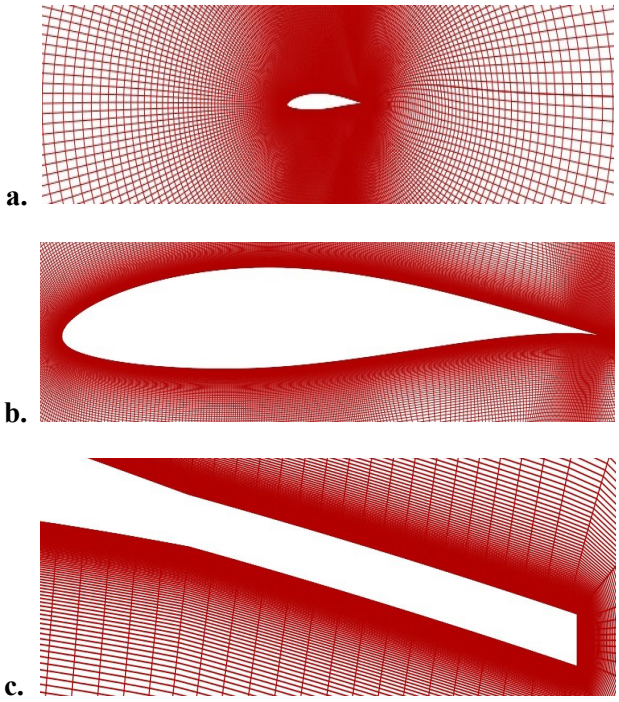

Figure 26. C81 Generator Airfoil Fitted O-grid: a.) Far-Field View, b.) Airfoil View, c.) Trailing Edge View

Table 1. C81 Generator – Airfoil Grid Resolution Study

Grid Number	Periodic Cells	Normal Cells	y+
1	201	101	0.5
2	301	151	0.5
3	401	201	0.5
4	501	251	0.5
5	601	301	0.5

STAR-CCM+ Model

This sub-section describes the progression of the STAR-CCM+ blade-element model. First was the single rotor model with hub, which takes the solidity of the coaxial rotor and places it all on one single rotor. This was done so as to start with the simplest practical CFD model that would then later be developed into its full complexity. The single and coaxial models use STAR-CCM+'s built-in blade-element method. This approach solves the RANS equations with k-ω omega turbulence. In this model, the user specifies the blade twist, chord, collective and cyclic control, and airfoil deck. The user also has the ability to specify azimuthal flapping and coning, as well as hinge offsets; however, the current coaxial non-articulated fixed-pitch rotors left many of the more advanced options unused. A GRS was carried out to strike a balance between cell-count and computational time, giving the final grid approximately 1.6 million cells. The rotor collective and RPM were set in an iterative manner. First, the coaxial model's RPM was trimmed with the design tip-pitch held constant in order to provide the required thrust for a pre-determined 1g-hover. Then, the single rotor's collective was trimmed to achieve the same thrust at the same RPM. This allowed for the ratio of thrust-coefficient to solidity, or C_T/σ, to be the same between the two models, which allows for a truly fair comparison of the figures of merit. Figures 27-28 show the single rotor grid and hover downwash velocity, respectively.

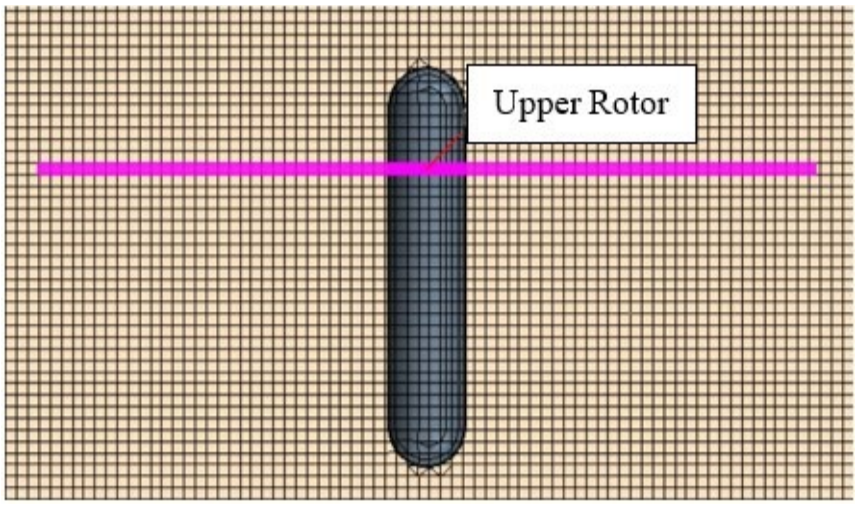

Figure 27. STAR-CCM+ Blade-Element Model Grid

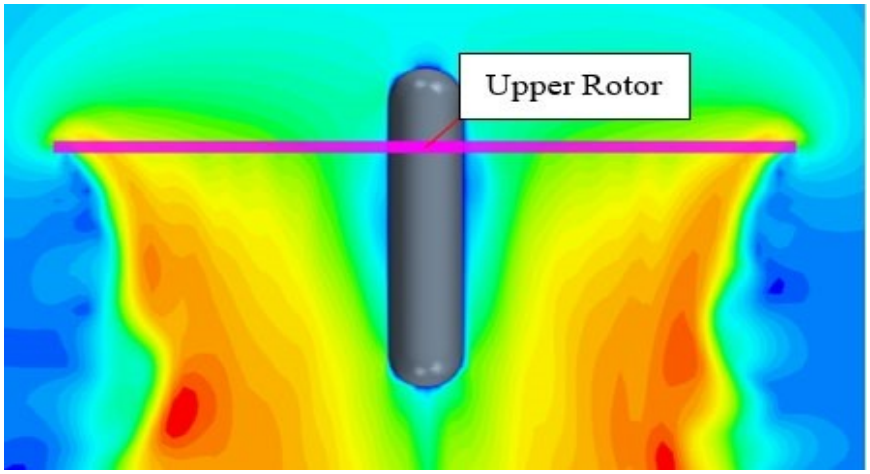

Figure 28. STAR-CCM+ Single Rotor Velocity

The coaxial rotor model keeps everything identical to the single rotor model, with the exception that the four blades are split into their respective upper and lower rotor positions. This means that the same solidity of the single rotor is now spread across the upper and lower rotors. The rotor-rotor separation was set to half of the rotor radius for the blade-element models. The model is now setup for the final counter-rotating coaxial design. Figure 29 shows a velocity plot of the rotor inflow and downwash in hover.

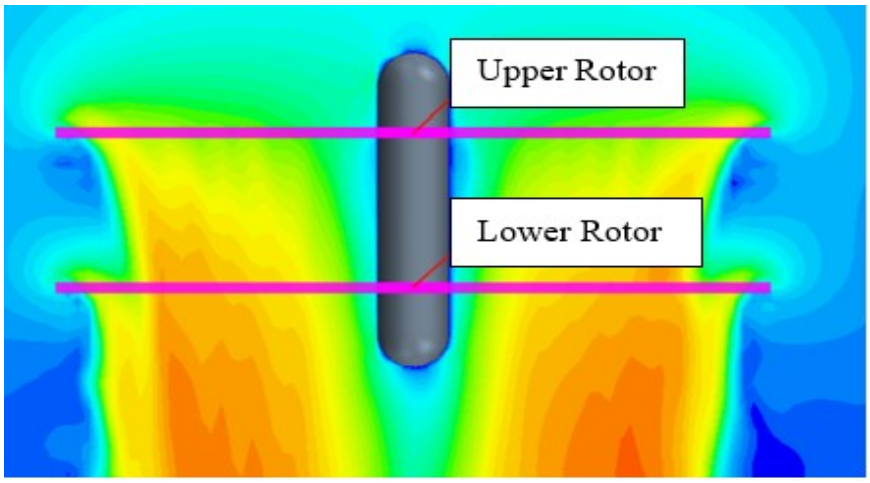

Figure 29. STAR-CCM+ Coaxial Rotor Velocity

RotCFD Model

A nearly identical process was carried out using the RotCFD toolset to develop a second blade-element model. This sub-section discusses the model development, the consistencies with the STAR-CCM+ model, and the differences. This will allow for a fair discussion of results and comparison of the two software approaches.

The RotCFD versions 401 and 402 were used in this work, specifically their RotUNS package. RotUNS is the unstructured solver included with RotCFD. The 3D solver provides a body-fitted meshing capability for accurate tessellation of 3D objects. Tetrahedral cells make up the near-body region, with a Cartesian grid mesher everywhere else. RotUNS is also a RANS solver with a realizable k-ϵ turbulence model.

The first RotCFD model developed was an isolated single rotor (i.e. without the hub). This means that the grid is fully Cartesian, allowing for shorter run times. The rotor parameters were kept the same as the STAR-CCM+ model in order to maintain the ability for a comparison of the two solutions. This model excluded the hub to allow for a simple first cut at the problem, to develop

the grid, and to later observe the hub's impact on rotor performance. Figures 30-32 show two views of the grid and a plot of the velocity.

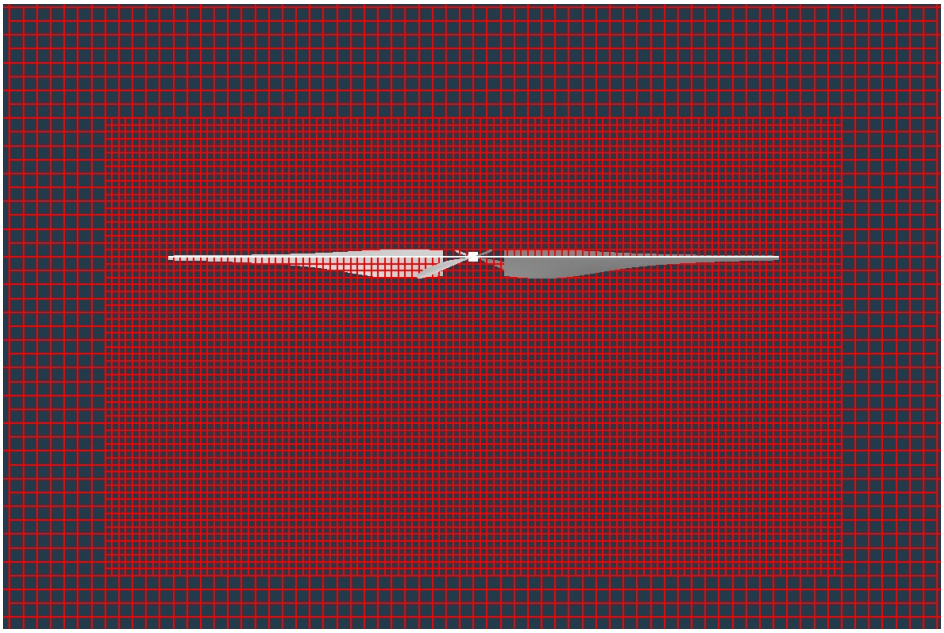

Figure 30. RotCFD Isolated Rotor Grid

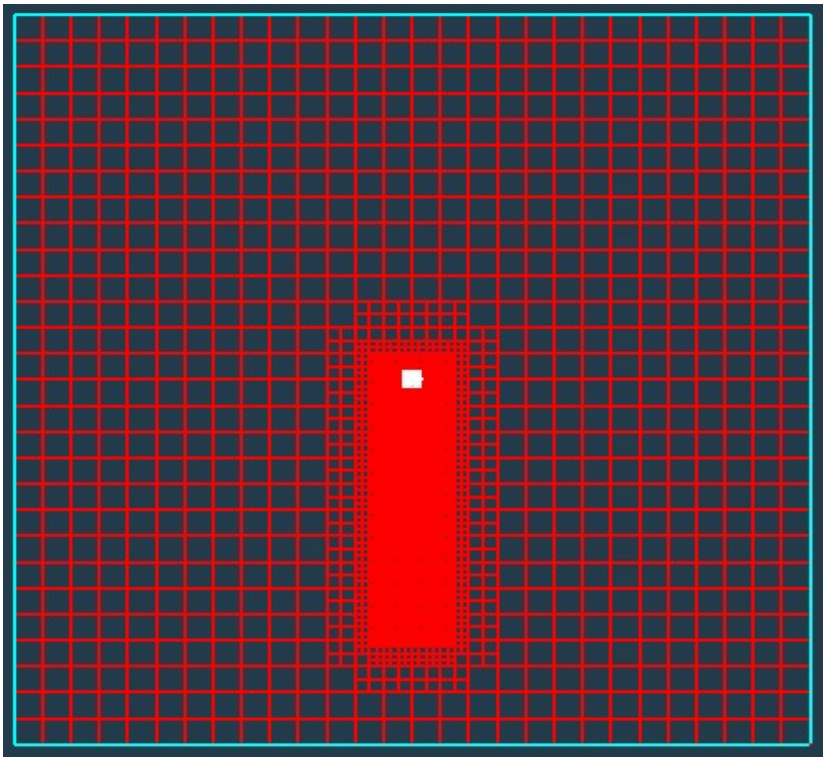

Figure 31. RotCFD Isolated Rotor Grid Wake Refinement

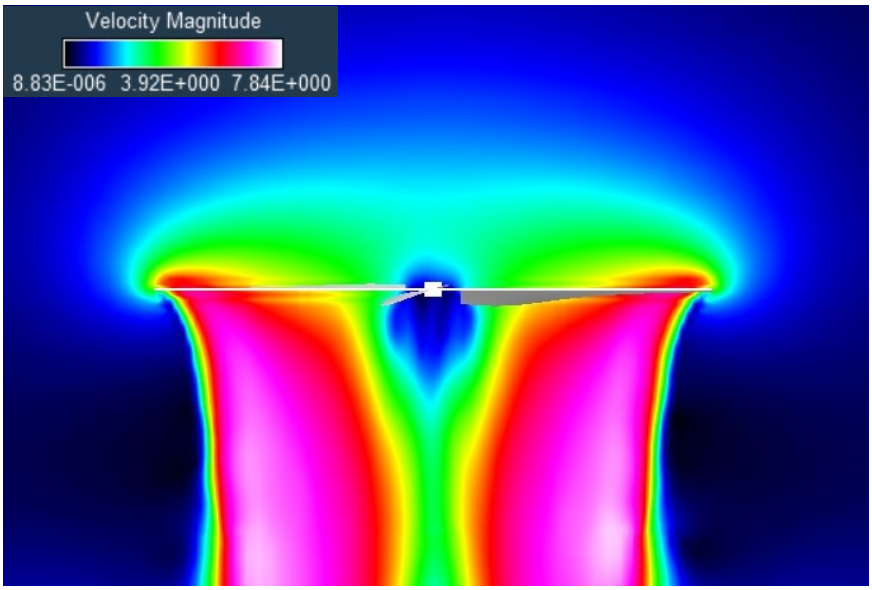

Figure 32. RotCFD Isolated Rotor Velocity

The next model added the same hub geometry that was used in the STAR-CCM+ models, but maintained the single rotor configuration. This allowed for a quantifiable comparison of the representative hub's impact on the rotor's performance. A time-step of 0.001 seconds was used, which achieved a Courant-Friedrichs-Lewy (CFL) number below 1. A subsequent GRS was carried out to determine the cell density required for an accurate simulation, while keeping the run time at about two hours on the workstation. The rotor collective and RPM were kept the same as the STAR-CCM+ single rotor values, so as to have a truly identical model setup for comparison of the two solution methods. Figures 33-34 show the single rotor's grid and a plot of the model's velocity in hover, respectively. The blade tip pitch (BTP) is also defined on the plots, since this was adjusted through the use of collective as described previously in the STAR-CCM+ Simulations section.

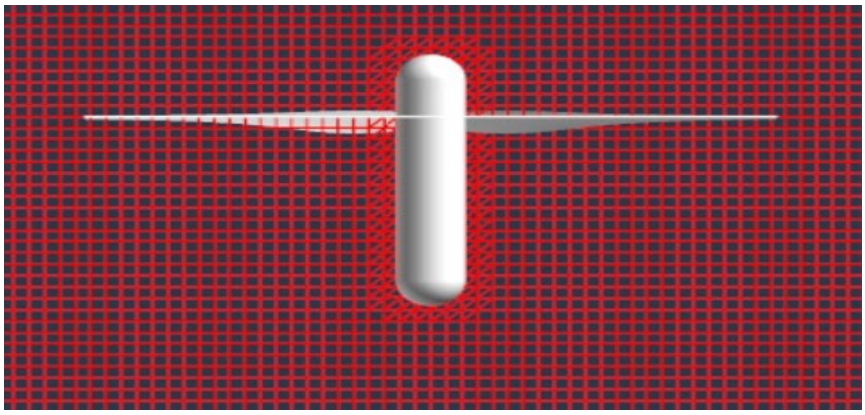

Figure 33. RotCFD Single Rotor Grid

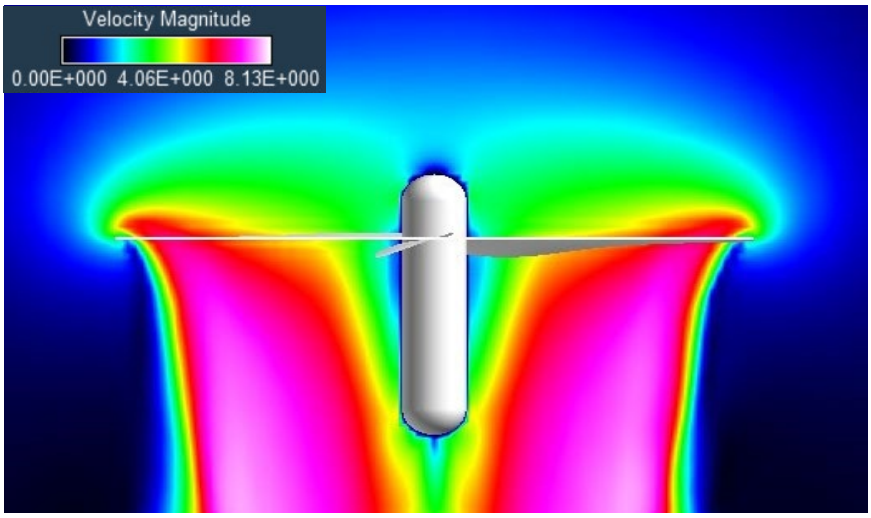

Figure 34. RotCFD Single Rotor Velocity, RPM = 600, BTP = 8.3 deg.

The creation of the coaxial model followed the same process as with the STAR-CCM+ model in that the only change was the division of the single rotor's solidity amongst the upper and lower counter-rotating pair. The rotor collective and RPM were set to the same values as the STAR-CCM+ coaxial values, which was 7 degrees BTP and 600 RPM. Figure 35 shows a plot of the coaxial rotor velocity. Figure 36 shows the lift coefficient versus blade radial position for both the upper and lower rotors. The deviation in lift coefficient can be understood by closely observing Figures 35 and 36 in unison. The lower rotor is seen operating in the wake of the upper rotor. From

momentum theory, the vena-contracta is known to be roughly 70% of its original area. This means that the inboard approximately 83% of the lower rotor is operating at a reduced angle-of-attack, which explains the reduced lift coefficient when compared to the upper rotor over that portion of the blade.

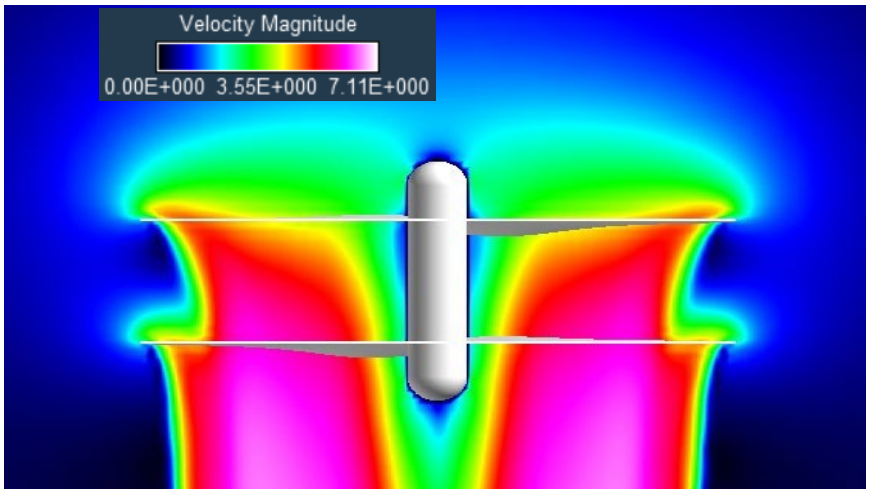

Figure 35. RotCFD Coaxial Rotor Velocity, RPM = 600, BTP = 7 deg.

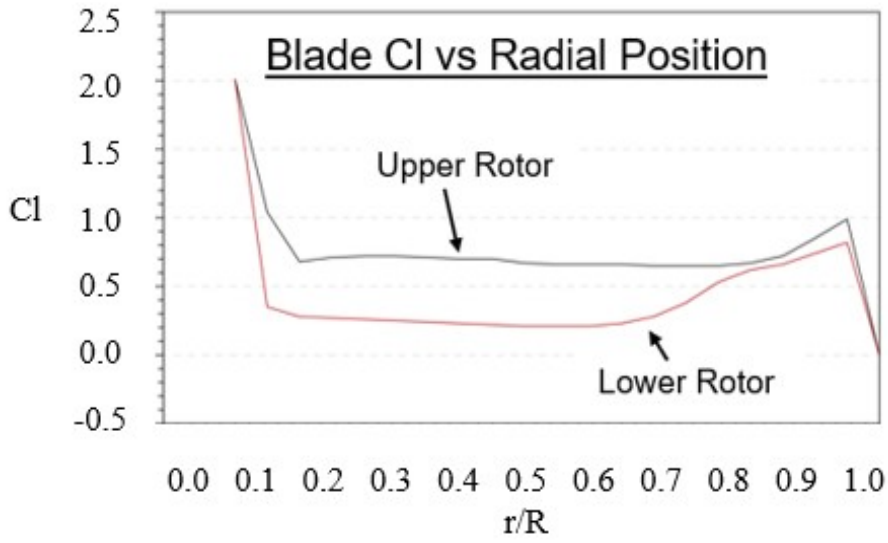

Figure 36. Lift Coefficient vs Blade Radial Position

Chapter 4

Results

The results are presented in the following order:

1.) Comparison of the blade-resolved mixing-plane model to the baseline time-accurate model.

2.) The blade-modeled comparison of the two blade-element models.

3.) RotCFD coaxial performance predictions.

Blade-Resolved Approach: Mixing-Plane Compared to Time-Accurate Model

Rotor performance metrics such as thrust, torque, and figure of merit (FM) have been gathered from both the novel mixing-plane and conventional time-accurate approaches. Information related to the computational models such as cell count and computational time have also been tracked. Figure 37 shows the total coaxial rotor thrust, individual rotor torques, total cell count, and computational time for the coarse time-accurate model (1.5-degree time-steps) versus the mixing-plane model; Figure 38 shows the same information for the refined time-accurate model (0.25-degree time-steps) versus the mixing-plane model. The cell count is plotted in millions and the computational time, which is defined as the number of physical hours the simulation was run multiplied by the number of cores, is plotted in thousands of hours. Tables 2-3 show the same information as Figures 37-38, respectively, along with additional parameters. The percentages shown in the figures and in the tables are percent differences between the two approaches, which is comparing the accuracy of the novel mixing-plane approach to the widely accepted time-accurate solution method.

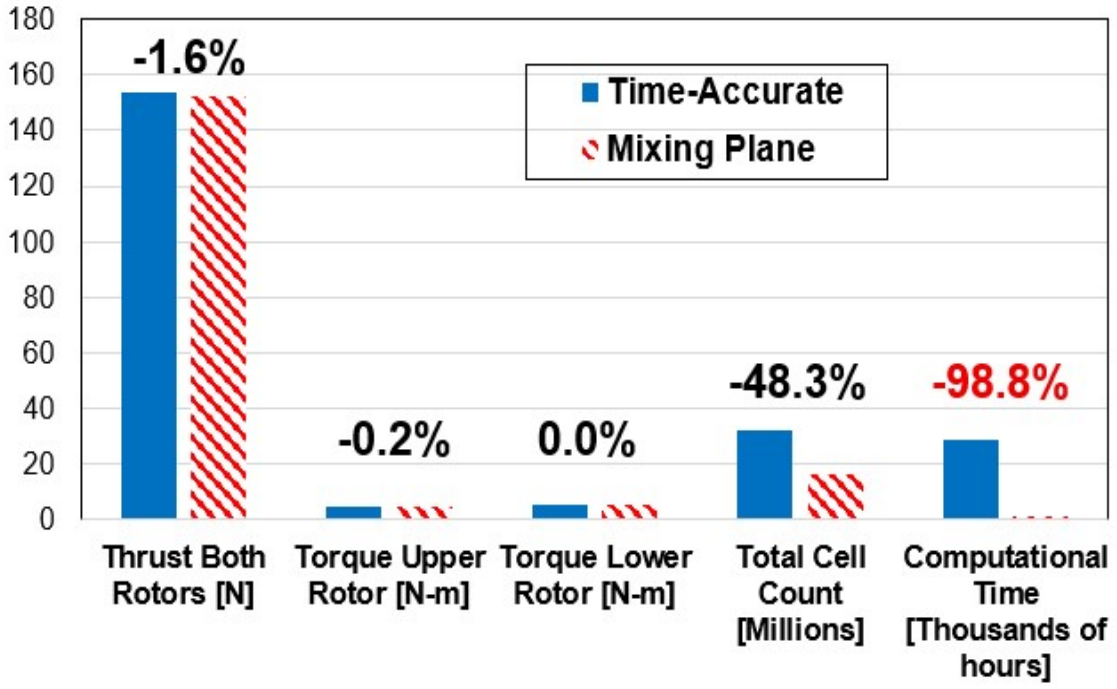

Figure 37. Results for Coarse Time-Accurate Model (1.5 Degree Time-steps) vs. Mixing-Plane Model

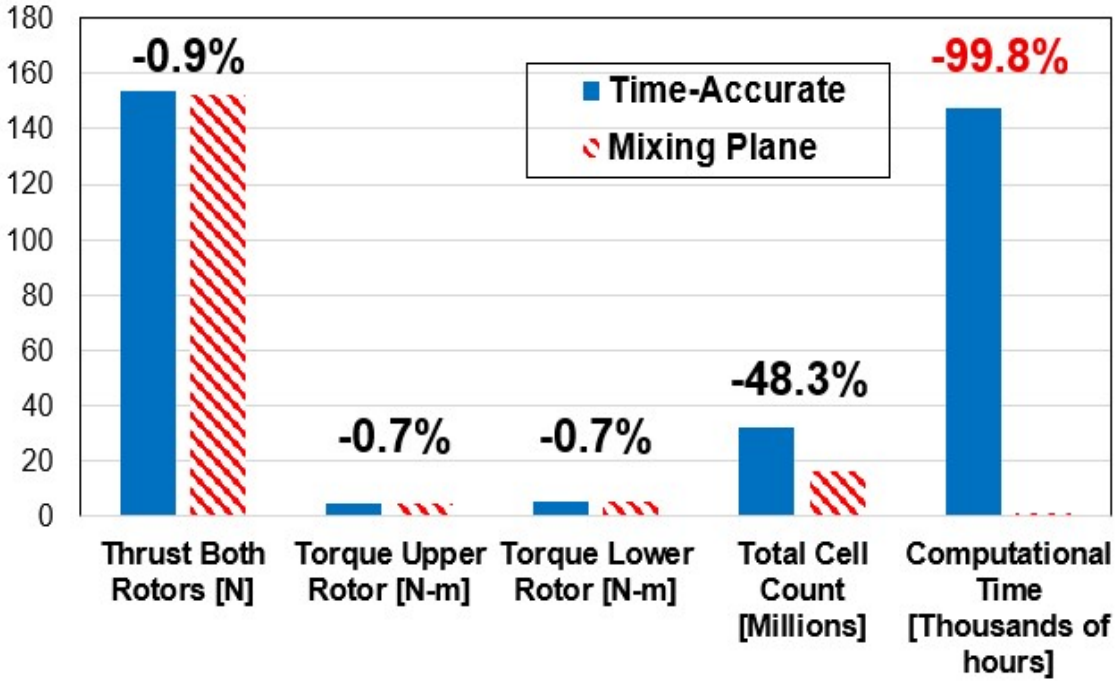

Figure 38. Results for Refined Time-Accurate Model (0.25 Degree Time-steps) vs. Mixing-Plane Model

Table 2. Results for Coarse Time-Accurate Model (1.5 Degree Time-steps) vs. Mixing-Plane Model

Model Parameter	Time-Accurate Model	Mixing-Plane Model	Percent Difference
Thrust Both Rotors	154.7 N	152.2 N	-1.6 %
Thrust Upper Rotor	79.9 N	78.2 N	-2.1 %
Thrust Lower Rotor	74.9 N	74.0 N	-1.2 %
Figure of Merit	0.773	0.755	-2.3 %
Torque Upper Rotor	4.43 N-m	4.42 N-m	-0.2 %
Torque Lower Rotor	5.52 N-m	5.52 N-m	0.0 %
Physical Blades	4	2	-50.0 %
Cell Count	31.9 M	16.5 M	-48.3 %
Computational Time	28,480 hr.	343 hr.	-98.8 %

Table 3. Results for Refined Time-Accurate Model (0.25 Degree Time-steps) vs. Mixing-Plane Model

Model Parameter	Time-Accurate Model	Mixing-Plane Model	Percent Difference
Thrust Both Rotors	153.6 N	152.2 N	-0.9 %
Thrust Upper Rotor	79.6 N	78.2 N	-1.8 %
Thrust Lower Rotor	74.0 N	74.0 N	0.0 %
Figure of Merit	0.767	0.755	-1.6 %
Torque Upper Rotor	4.45 N-m	4.42 N-m	-0.7 %
Torque Lower Rotor	5.48 N-m	5.52 N-m	0.7 %
Physical Blades	4	2	-50.0 %
Cell Count	31.9 M	16.5 M	-48.3 %
Computational Time	147,587 hr.	343 hr.	-99.8 %

Blade-Modeled Approach: Comparison of Blade-Element Models

Rotor performance metrics such as thrust coefficient, power/torque coefficient, and FM have been tabulated for both the single rotor model and coaxial rotor model for the two different CFD programs. Table 4 shows the percent deviation for these metrics between the RotCFD and STAR-CCM+ simulations. The largest deviation is observed to be less than three percent, showing confidence in the validity of the hover simulations.

As for forward flight, Figures 39-40 show the total coaxial rotor thrust and power vs RPM for both the STARCCM+ and RotCFD models at a forward flight design point of 12.5 mps flight speed with a 15-degree forward shaft angle. An offset is observed in Figure 39 with the STAR-CCM+ predicted thrust consistently higher than that of the RotCFD model. Comparing these predictions to theoretical calculations from Leishman, Ref. 27-28, and a conventional time-accurate CFD simulation of the same coaxial rotor by Kinzel et al., Ref. 29, shows the RotCFD blade-element model to closely predict the correct thrust in forward flight. The discrepancy observed for current STAR-CCM+ results is the subject of further studies.

Table 4. Comparison of RotCFD and STAR-CCM+ Blade-Element Models

Software and Model	CT	CP	FM
RotCFD Single Rotor	0.016619	0.001969	0.769238
STAR-CCM+ Single Rotor	0.016467	0.001996	0.748497
Percent Difference Single Rotor Models	0.9%	-1.4%	2.8%
RotCFD Coaxial Rotor (1.3 M cells)	0.016233	0.001703	0.858842
STAR-CCM+ Coaxial Rotor (1.6 M cells)	0.016280	0.001676	0.876453
Percent Difference Coaxial Rotor Models	-0.3%	1.6%	-2.0%

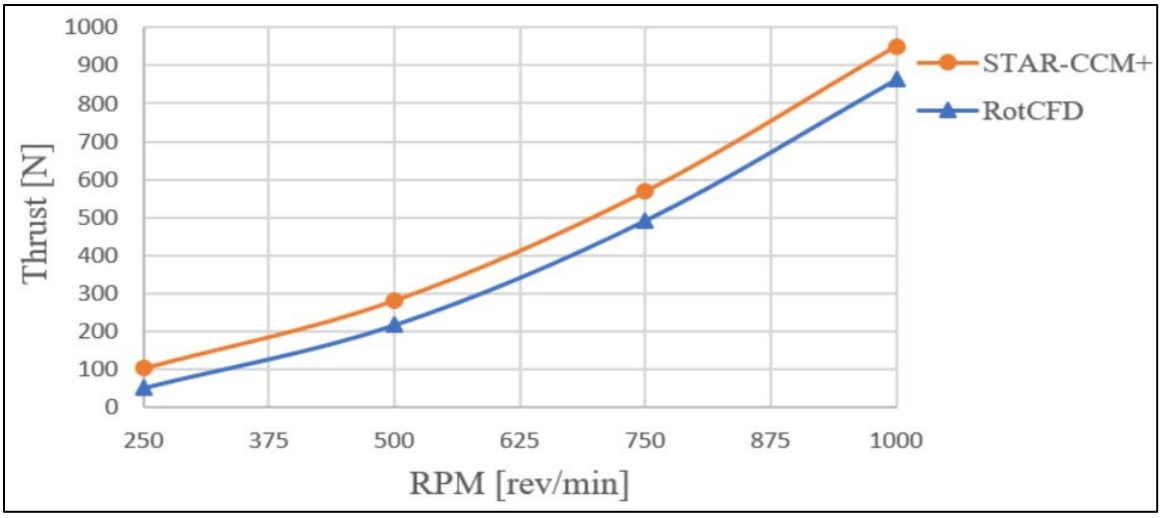

Figure 39. Thrust vs RPM Comparison for RotCFD and STAR-CCM+,
12.5 mps Forward Flight Speed, 15 deg. Forward Shaft Tilt

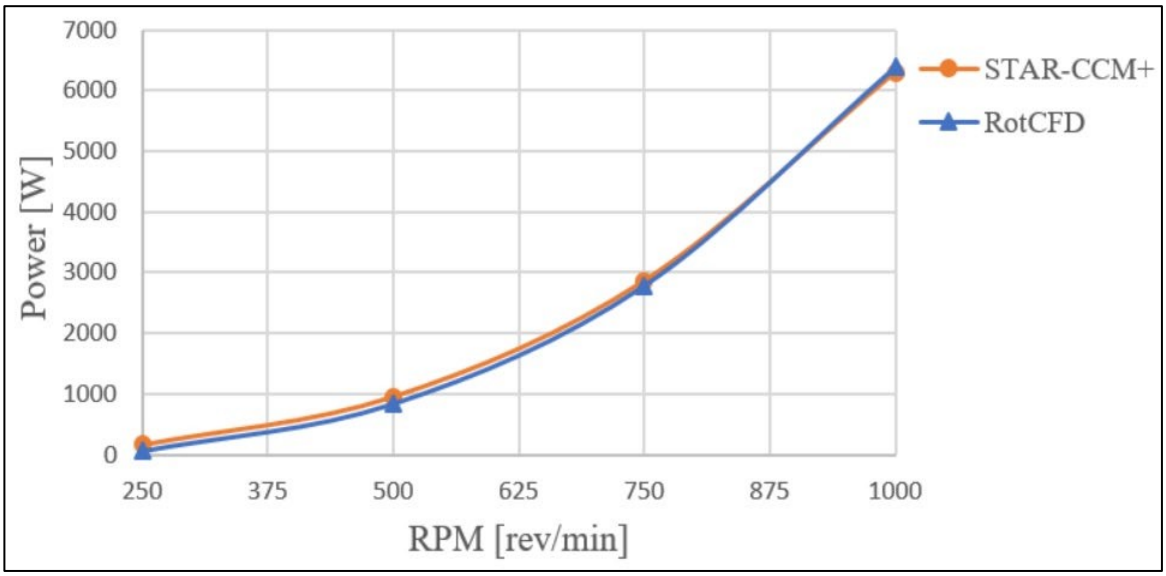

Figure 40. Power vs RPM Comparison of STAR-CCM+ and RotCFD,
12.5 mps Forward Flight Speed,15 deg. Forward Shaft Tilt

Blade-Modeled Approach: Performance Predictions of a Coaxial Rotor

Figures 41-43 plot the thrust, power, and FM of the RotCFD coaxial rotor model as a function of RPM. The charts show the upper rotor values, the lower rotor values, and the total

coaxial rotor values. The thrust and power are summarized in Table 5. Figures 44-45 show the RotCFD thrust and power vs RPM at various axial climb speeds.

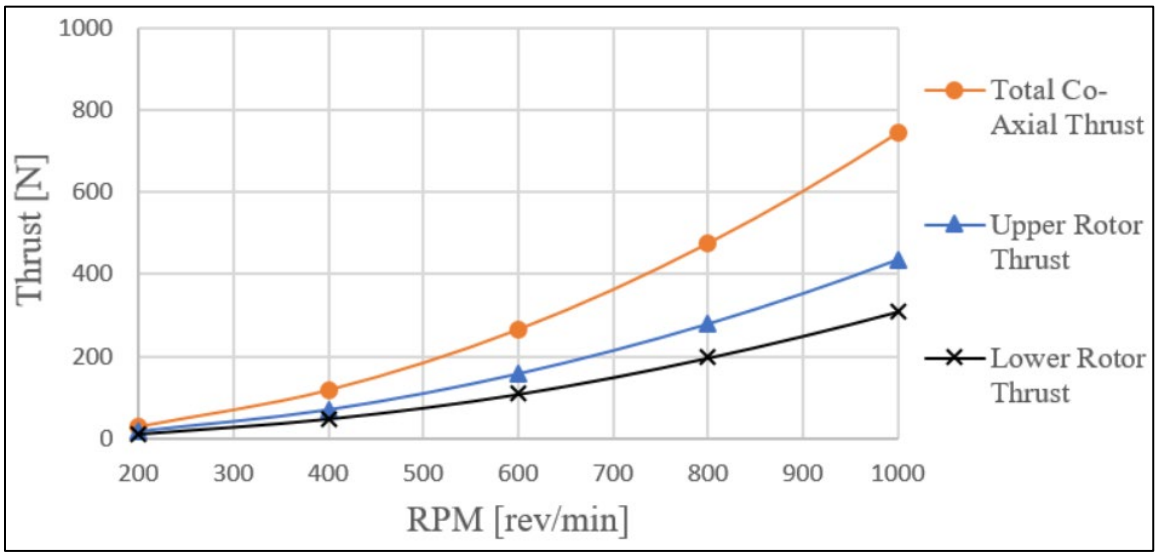

Figure 41. RotCFD Coaxial Rotor Thrust vs RPM in Hover

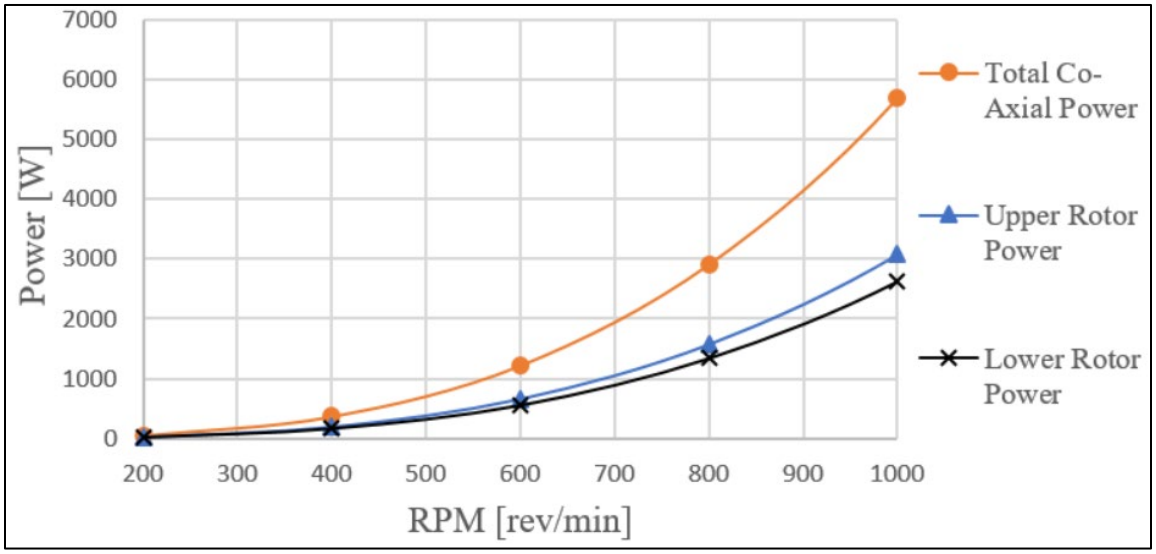

Figure 42. RotCFD Coaxial Rotor Power vs RPM in Hover

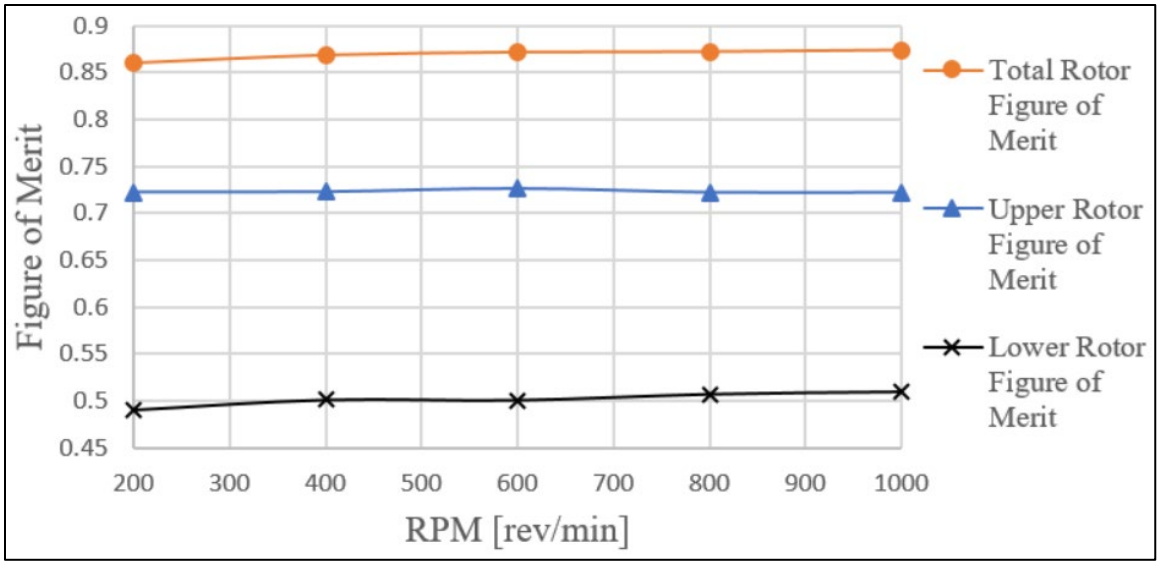

Figure 43. RotCFD Coaxial Rotor FM vs RPM in Hover

Table 5. RotCFD Coaxial Hover RPM Sweep

RPM	Total Thrust (N)	Total Power (W)
200	29	46
400	118	363
600	266	1219
800	475	2913
1000	744	5698

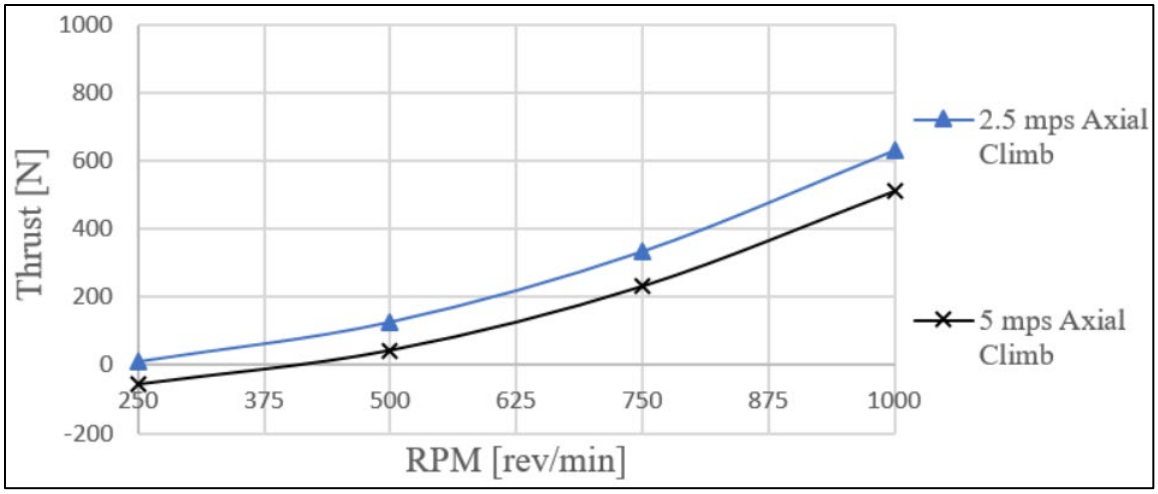

Figure 44. RotCFD Coaxial Rotor Thrust vs RPM in Axial Climb

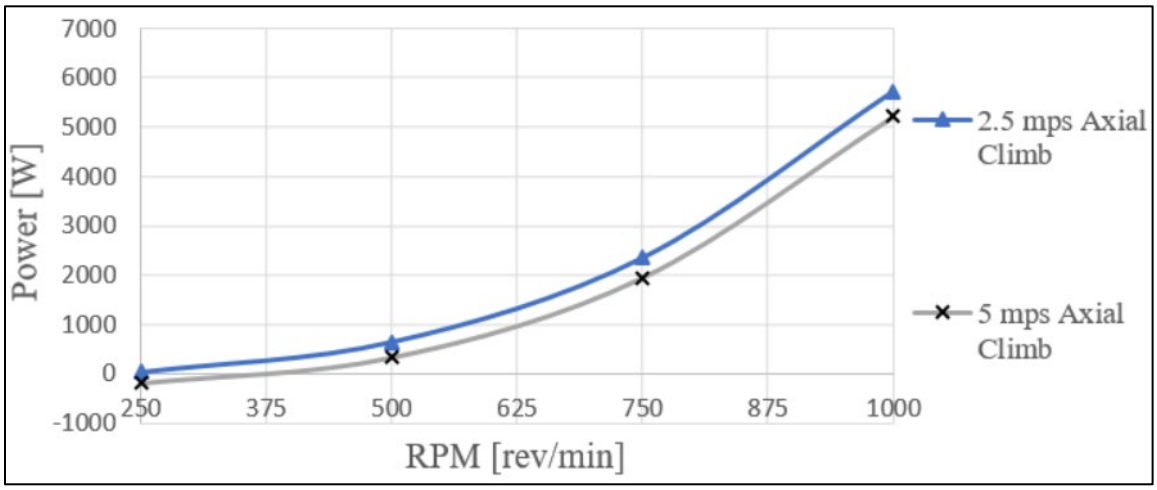

Figure 45. RotCFD Coaxial Rotor Power vs RPM in Axial Climb

The RotCFD blade-element model was also used to analyze a motor-out condition. The goal was to determine the RPM increase required in the event of a single motor failure to maintain 1-g hover. A baseline model, Figure 46, was created by simply removing the lower rotor, which meant that the upper rotor had half the solidity of all the rotor models discussed up to this point. The second model, Figure 47, had the lower rotor included, but it was held stationary as it would be in a true lower rotor failure. Lastly in Figure 48, the upper rotor was held stationary while the

lower rotor generated the thrust. The RPM in each case was trimmed with the rotor design's BTP of 7 degrees to achieve the thrust required for 1g-hover. An approximate 7% increase in RPM was required with the addition of the stationary lower rotor when compared to the simplified removed rotor model. Furthermore, the upper motor-out condition is observed to require less RPM than the lower motor-out condition, which is due to the downloading experienced in the lower motor-out case. It is noted that the most extreme case, a lower motor failure, requires a 34% increase in RPM over the nominal coaxial case to maintain the 1-g hover thrust.

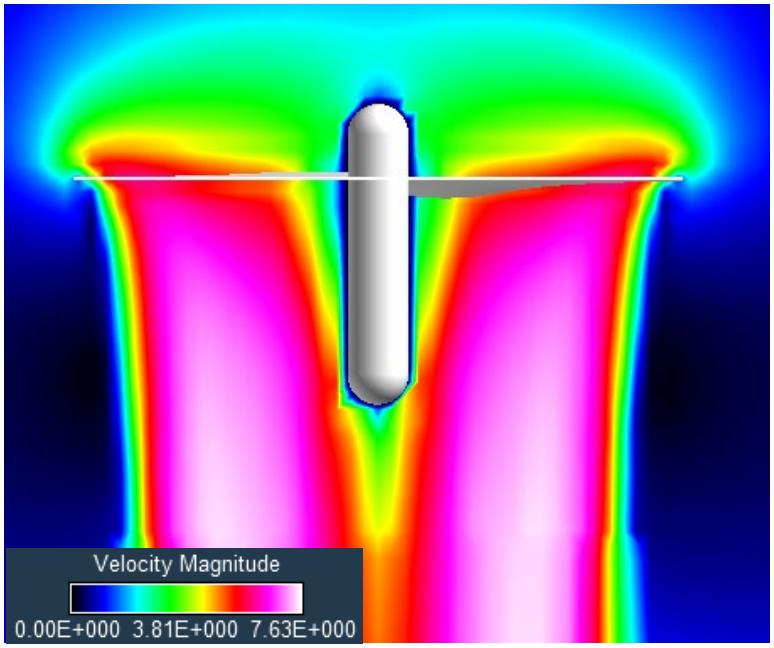

Figure 46. Motor-Out Simplified Condition, Upper Rotor 1g-Hover, RPM = 755, BTP = 7 deg., Lower Rotor Removed

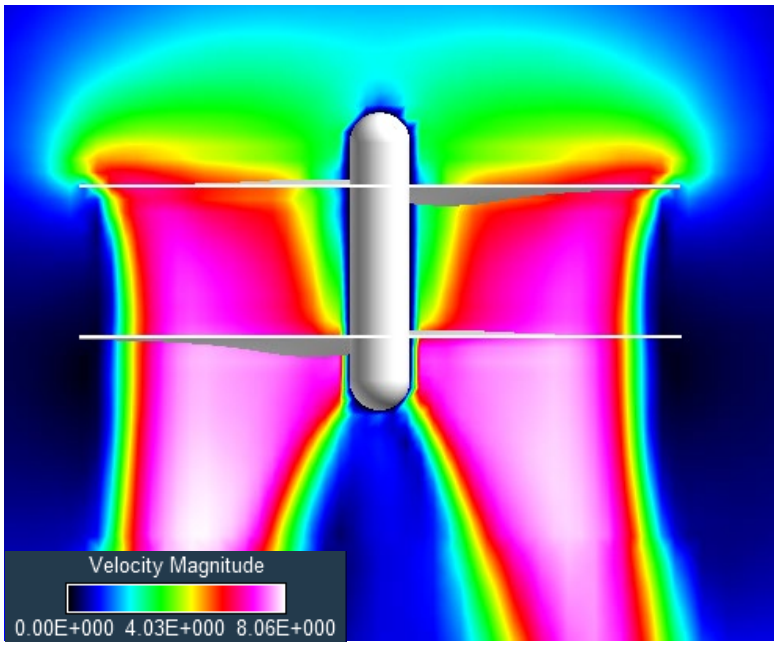

Figure 47. Motor-Out Condition, Upper Rotor 1g-Hover, RPM = 805, BTP = 7 deg., Lower Rotor Stationary

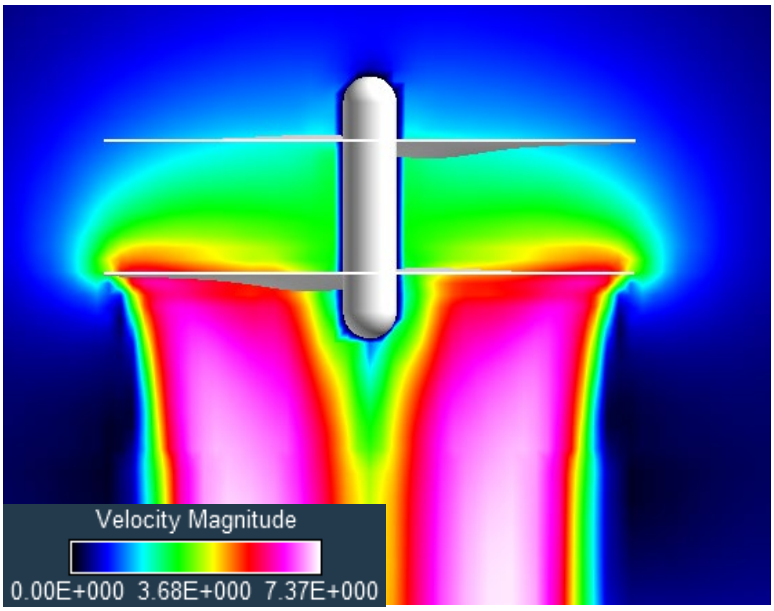

Figure 48. Motor-Out Condition, Lower Rotor 1-g Hover, RPM = 745, BTP = 7 deg., Upper Rotor Stationary

Chapter 5

Summary and Future Work

The objectives of this thesis were to:

1.) Develop an efficient blade-resolved approach for multicopter analysis in hover.

2.) Create a blade-modeled approach for analysis of multicopter rotors in various flight conditions.

3.) Use the blade-modeled approach to analyze a coaxial rotor configuration.

Two CFD approaches for the efficient analysis of multicopter UAS have been studied. The first, suitable for steady state hover, incorporates a novel blade-resolved approach using mixing-plane boundaries that allow for the use of periodic boundaries, rotating reference frames, and a steady RANS solver. Theoretical calculations were used in conjunction with grid-refinement studies throughout the development of the model to optimize the grid parameters. This resulted in a high-fidelity grid capable of capturing the relevant aspects of the rotor system.

The same grid parameters were used to create a conventional, state-of-the-art, time-accurate model. It has roughly twice the number of cells since all four blades are resolved, as opposed to just two with the periodic boundaries of the mixing-plane model. Results were presented comparing the rotor performance between the conventional time-accurate model and the novel mixing-plane approach. The time-accurate model was run once with coarse 1.5-degree time-steps and once with refined 0.25-degree time-steps. The results comparing the refined time-accurate model with the mixing-plane model show the largest deviation of rotor performance metrics to be the upper rotor thrust at 1.8%. The computational time to arrive at this result was reduced by 99.8%. This is a 430 times reduction in computational time, or more than two orders-of-magnitude. In the present research, this meant getting the rotor performance data, matching

within less than 2% of the state-of-the-art calculations, in two hours on 160 cores instead of more than two and a half weeks on 320 of the same cores. Although there are applications where the extra 2% fidelity is required, this approach provides a good solution for rapid configuration testing and engineering design in a fraction of the time. Once a near-final design is closed in on, the higher-fidelity tools can then be incorporated into the analysis if they are required. This also brings a high-fidelity analysis tool within reach for those without large computational resources. Running on a desktop computer with 16 or 32 cores, for example, would result in the same solution with a still manageable run time.

Another benefit observed in the mixing-plane model is the largely reduced overall cell count, which was a 48.3% reduction. This was realized through the use of periodic boundaries, which the mixing-plane approach allows for even in a coaxial simulation. Mixing-plane simulations were thus run on half the number of cores as compared to the time-accurate approach, which also contributes to the time savings since there is less communication required between nodes on the cluster.

A second CFD model was also developed, in order to analyze forward flight conditions in addition to hover and axial flight, using a blade-modeled approach. Single rotor and coaxial rotor models were simulated. Solutions for the rotor models from two independent CFD solvers, STAR-CCM+ and RotCFD, have been shown to agree within 3% for thrust coefficient, power coefficient, and FM in the design hover case. The RotCFD coaxial rotor model, which also compared well with theoretical calculations and a conventional state-of-the-art time-accurate model in forward flight, has been used to analyze the current coaxial rotor design in edge-wise forward flight, axial climb, and motor-out conditions.

This research has made progress towards its goal to create a set of efficient analysis tools

for the optimization of multicopter UAS, and the insights gained can potentially increase design capabilities for future multicopter aeronautical concepts. Future work exists in extending the approach to forward flight. This would allow for the same efficient blade-resolved rotor simulations in forward flight, and open the door for highly efficient coaxial and multicopter analyses in the various flight conditions pertinent to vehicle design. Future research interests also lie in furthering the development of efficient CFD methods as they pertain to the coupling of CFD with computational structural dynamics, or CFD-CSD coupled simulations. This would involve the tight coupling of blade-resolved CFD analysis with a CSD solver in order to accurately capture the unsteady aeroelastic effects taking place due to deformation of the rotor blades.

References

1. Young, L. A., "Conceptual Design Aspects of Three General Sub-Classes of Multi-Rotor Configurations: Distributed, Modular, and Heterogeneous," The 6th AHS Specialists Meeting on Unmanned Rotorcraft Systems, Scottsdale, Arizona, Jan. 2015.
2. Russell, C., Jung, J., Willink, G., and Glasner, B., "Wind Tunnel and Hover Performance Test Results for Multicopter UAS Vehicles," The 72nd AHS Annual Forum, West Palm Beach, Florida, May 2016.
3. Gregory, D., Cornelius, J., Waltermire, S., Loob, C., Schatzman, N., "Acoustic Testing of Five Multicopter UAS in the U.S. Army 7- by 10-Foot Wind Tunnel," NASA/TM–2018–219894, Nov. 2018.
4. Barbely, N., Komerath, N., Novak, L., "A Study of Coaxial Rotor Performance and Flow Field Characteristics," American Helicopter Society Technical Meeting on Aeromechanics Design for Vertical Lift Proceedings, San Francisco, CA, January 2016.
5. Yoon, S., Lee, H. C., Pulliam, T. H., "Computational Analysis of Multi-Rotor Flows," AIAA Paper 2016-0812, The 54th AIAA Aerospace Sciences Meeting, San Diego, California, Jan 4-8, 2016.
6. Yoon, S., Lee, H., Pulliam, T., "Computational Study of Flow Interactions in Coaxial Rotors," American Helicopter Society Technical Meeting on Aeromechanics Design for Vertical Lift Proceedings, San Francisco, CA, January 2016.
7. Yoon, S., Chan, W. M., and Pulliam, T. H., "Computations of Torque-Balanced Coaxial Rotor Flows," AIAA Paper 2017-0052, The 55th AIAA Aerospace Sciences Meeting, Gaylord, Texas, Jan. 2017.

8. Yoon, S., Diaz, P., Boyd, D., Chan, W., Theodore, C., "Computational Aerodynamic Modeling of Small Quadcopter Vehicles," American Helicopter Society 73rd Annual Forum Proceedings, Fort Worth, TX, May 2017.
9. Strawn, R., Caradonna, F., Duque, E., "30 Years of Rotorcraft Computational Fluid Dynamics Research and Development," Journal of the American Helicopter Society, Volume 51, Number 1, January 2006.
10. Gray, R. B., "An Aerodynamic Analysis of a Single Bladed Rotor in Hovering and Low Speed Forward Flight as Determined from Smoke Studies of the Vorticity Distribution in the Wake," Technical Report No. 356, Princeton University, 1956.
11. Potsdam, M. A., Strawn, R. C., "CFD Simulations of Tiltrotor Configurations in Hover," Journal of the American Helicopter Society, Vol. 50, (1), 2005.
12. Aftosmis, M. J., Berger, M. J., and Melton, J. E., "Robust and Efficient Cartesian Mesh Generation for Component-Based Geometry," AIAA Journal, Vol. 36, 1998.
13. Lee-Rausch, E., Biedron, R., "FUN3D Airloads Predictions for the Full-Scale UH-60A Airloads Rotor in a Wind Tunnel," Journal of the American Helicopter Society, Volume 59, Number 3, July 2014.
14. Ahaus, L., Makinen, S., Meadowcroft, T., Tadghighi, H., Sankar, L., Baeder, J., "Assessment of CFD/CSD Analytical Tools for Improved Rotor Loads"
15. Collins, K., Lakshmi, S., Dimitri, M., "Application of Low- and High-Fidelity Simulation Tools to Helicopter Rotor Blade Optimization," Journal of the American Helicopter Society, Volume 58, Number 4, October 2013.

16. Schmitz, S., Bhagwat, M., Moulton, M., Caradonna, F., Chattot, J., "The Prediction and Validation of Hover Performance and Detailed Blade Loads," Journal of the American Helicopter Society, Volume 54, Number 3, July 2009.
17. Siemens, "User Guide: STAR-CCM+ Version 12.06," (2017).
18. Sukra Helitek, "RotCFD: Rotor Computational Fluid Dynamics Integrated Design Environment."
19. Rajagopalan, G., Thistle, J., Polzin, W., "The Potential of GPU Computing for Design in RotCFD," AHS Technical Meeting on Aeromechanics Design for Vertical Lift, San Francisco, CA, January 16-18, 2018.
20. Spalart, P., Allmaras, S., "A one-equation turbulence model for aerodynamic flows," Paper AIAA 30th Aerospace Sciences Meeting and Exhibit, Reno, NV, Jan 6, 1992.
21. Mathur, S. R., Murthy, J. Y., "A Pressure-based Method for Unstructured Meshes," Numerical Heat Transfer, Vol. 31, (2), 1997, pp 195-215. Doi: 10.1080/10407799708915105
22. Drela, M., "XFOIL: An Analysis and Design System for Low Reynolds Number Airfoils," Low Reynolds Number Aerodynamics, Springer, Berlin, Heidelberg, 1989, pp 1-12.
23. Abbott, I. H., and Von Doenhoff, A. E., Theory of Wing Sections: Including a Summary of Airfoil Data, National Advisory Committee for Aeronautics, Langley, VA, 1945, pp. 146.
24. Schmitz, S., "XTurb-PSU A Wind Turbine Design and Analysis Tool," The Pennsylvania State University, 2012.
25. NASA Ames Research Center, "ARC2D (Efficient Two-Dimensional Solution Methods for The Navier-Stokes Equations)."

26. Koning, W. J. F., Johnson, W., Allan, B. G., "Generation of Mars Helicopter Rotor Model for Comprehensive Analyses," AHS Technical Meeting on Aeromechanics Design for Vertical Lift, San Francisco, CA, January 16–18, 2018.

27. Leishman, J. G., Principles of Helicopter Aerodynamics, Cambridge University Press, New York, NY, 2000, Chapter 10.

28. Leishman, J. G., Ananthan, S., “Aerodynamic Optimization of a Coaxial Proprotor,” American Helicopter Society 62nd Annual Forum Proceedings, Phoenix, AZ, May 9-11, 2006.

29. Kinzel, M., Cornelius, J., Schmitz, S., Palacios, J., Langelaan, J., Adams, D., Lorenz, R., “An Investigation of the Behavior of a Coaxial Rotor in Descent and Ground Effect,” AIAA SciTech Forum, 7-11 January 2019, San Diego, CA.

Jason K. Cornelius

NSF Graduate Research Fellow
Department of Aerospace Engineering
The Pennsylvania State University, University Park, PA 16802
Phone: 570-332-2300 Email: joc5693@psu.edu

Education

Master of Science, Aerospace Engineering — GPA: 3.72/4.00
The Pennsylvania State University, — May 2019

Bachelor's Degree, Aerospace Engineering, Minor in Russian — GPA: 3.86/4.00
Schreyer Honors College, The Pennsylvania State University, — August 2018

Professional Experience

Aug. 2018-Present **NSF Graduate Research Fellow**
Department of Aerospace Engineering,
The Pennsylvania State University

July 2018-Aug. 2018 **Rotorcraft Aeromechanics Intern**
Aeromechanics Branch,
NASA Ames Research Center

Aug. 2016-Aug. 2018 **Undergraduate Researcher**
Undergraduate Thesis: "An Efficient CFD Approach for Co-Axial Rotor Simulations"

June-Aug. 2017 **Rotorcraft Aeromechanics Intern**
Aeromechanics Branch,
NASA Ames Research Center

June-Aug. 2016 **CFD Intern**
Flight Technology Research and Development Group,
Bell Helicopter

Jan.-April 2016 **Rotorcraft Aeromechanics Intern**
Aeromechanics Branch,
NASA Ames Research Center

May-Aug. 2015 **Rotorcraft Analysis Intern**
Mechanical Analysis Group,
Bell Helicopter

Jan. 2015 **Bell Helicopter Boot Camper**
Student Program Participant,

Bell Helicopter

June-Aug. 2014 **Undergraduate Research Assistant**
Vertical Lift Research Center of Excellence,
The Pennsylvania State University

Teaching Experience

Aug. 2018-Present **Teaching Assistant**
KINES 45: NAUI Basic SCUBA
The Pennsylvania State University

May-June 2016 **International Teaching Assistant**
ENGR 118: Impact of Culture on Engineering in China,
The Pennsylvania State University

June 2014-May 2015 **Teaching Assistant**
EDSGN 497K: Advanced CAD, CATIA
EDSGN 100: Introduction to Engineering Design, Solidworks
The Pennsylvania State University

Research Interests

Computational Fluid Dynamics
RANS/BEM approaches for optimization of multicopter aircraft
Mixing-plane boundaries in hover cases for reduction in computational cost

Experimental Wind Tunnel Testing

Small-Scale Wind Energy
Blade and rotor design
Electronic control of active pitch system
Systems integration of aerodynamic, mechanical, electrical, and control components

Publications, Presentations, and Reports

Jan. 2019 **AIAA SciTech, An Efficient CFD Approach for Co-Axial Rotor Simulations**

Nov. 2018 **NASA/TM–2018–219894, Acoustic Testing of Five Multicopter UAS in the U.S. Army 7- by 10-Foot Wind Tunnel**

Aug. 2018 **NASA, Simulating the Dragonfly Aircraft with RotCFD and STAR-CCM+**

Aug. 2017 **NASA, CFD Analysis of the Mars Parachute Testing in the NFAC Wind Tunnel**

April 2017 **Penn State Exhibition, Development of a CFD Prediction Tool for Planetary**

	Rotorcraft
Sept. 2016	**SAE International Powered Lift Conference, Closing the Speed Gap: A Novel Commercial Transonic VTOL Concept**
April 2016	**NASA, Acoustic Analysis of Multicopter UAS**

Awards and Honors

Fall 2018	**National Science Foundation Graduate Research Fellowship Program**
Fall 2018	**NASA Aeronautics Directorate Spotlight Award**
Spring 2018	**AHS Vertical Flight Foundation Bell Helicopter Scholarship**
Jan. 2018	**AHS Robert L. Lichten Mid-East Regional Competition Winner**
Fall 2017	**Foreign Language and Area Studies (FLAS) Fellowship**
Spring 2018	**Miller-Arm Endowment**
Spring 2018	**Penn State College of Engineering International Travel Grant**
Spring 2018	**Penn State Education Abroad Whole World Scholarship**
Spring 2018	**The Pennsylvania State University CIEE Scholarship**
Spring 2018	**CIEE Global Access Initiative**
Fall 2017	**Penn State Engineering Alumni Society Scholarship**
Spring 2017	**Goldwater Scholarship Honorable Mention**
Spring 2017	**US Naval Academy Leadership Conference: Schreyer Honors College Representative**
Spring 2017	**College of Engineering Research Initiative (CERI) Student**
Fall 2016	**Penn State Susson Trustee Scholarship**
Fall 2017	**Phi Kappa Psi Foundation District Scholarship**
Fall 2016	**AHS Vertical Flight Foundation Eugene K. Liberatore Scholarship**
Fall 2016	**NASA Pennsylvania Space Grant Undergraduate Scholarship**
Fall 2016	**Penn State Engineering Alumni Society Scholarship**
Fall 2016	**Phi Kappa Psi Foundation Jerry Nelson Award**
Fall 2016	**Phi Kappa Psi Foundation District Scholarship**
Spring 2016	**Sigma Gamma Tau National Aerospace Engineering Honor Society Inductee**

Fall 2015 **Department of Aerospace Engineering Lou Borges Scholarship**

Fall 2015 **Tau Beta Pi National Engineering Honor Society Inductee**

Fall 2014 **Boeing Company Scholarship**

Summer 2014 **Penn State College of Engineering International Travel Grant**

Fall 2013 **Penn State College of Engineering White Trustee Scholarship**

Fall 2013 **The President's Freshman Award**

Fall 2012 **Mountain Top Martial Arts Rank of Shodan (Black Belt)**

Professional Memberships

American Helicopter Society (AHS), member since 2013

American Institute of Aeronautics and Astronautics (AIAA), member since 2014

Organizations

Current

Penn State Wind Energy Club – Founder, Graduate Advisor

Penn State Russian Club

Penn State Pingers Toastmasters Club

Prior Roles

Penn State Vertical Flight Society (VFS) – Vice-President

Department of Energy Collegiate Wind Competition – Team Lead/ Aerodynamics Lead

Phi Kappa Psi Fraternity – Pledge Class President/ Academic Chair

AIAA Design Build Fly Competition – Team Lead

Skills

Aerospace Specific Skills

STAR-CCM+, RotCFD, MATLAB, Linux, ANSYS-FEA/FENSAP, FieldView, Tecplot, XFoil, X-Turb, WT_Perf, CATIA, SolidWorks, BEMT-Design, ICEM, 3D-Printing, Soldering, Electronics

Language and International Experience

Russian ACTFL - Advanced Mid Rating
ILR - Limited Working Proficiency
Intensive Semester-long Russian Language Program, St. Petersburg State University, St. Petersburg, Russia, Spring 2018
Penn State Embedded Program, Moscow Higher School for Economics, Moscow, Russia, Spring 2019

Chinese Chinese 2 – Penn State University, Spring 2019
Study Abroad Program, ENGR 118: Impact of Culture on Engineering in China, The Pennsylvania State University, Summers 2014 and 2016

Spanish High School Language Classes

Certifications

AAUS Science Diving (SCUBA)

Diving Certifications: NAUI Advanced, Rescue, Nitrox, Deep; PADI Open Water

Red Cross CPR, AED, and First Aid; DAN Diving First Aid for Professional Divers

Portfolio: https://drive.google.com/file/d/0Bygpc4Aqwr2SaVZXMnBFR1czZGc/view

LinkedIn: https://www.linkedin.com/in/jason-k-cornelius